Environmental and epigenetic regulation of *Rider* retrotransposons in tomato

Matthias Benoit[1, 6], Hajk-Georg Drost[1], Marco Catoni[1, 3], Quentin Gouil[2, 4], Sara Lopez-Gomollon[2], David Baulcombe[2] and Jerzy Paszkowski[1, 5, 6]

Affiliation

[1] The Sainsbury Laboratory, University of Cambridge, Cambridge CB2 1LR, United Kingdom

[2] Department of Plant Sciences, University of Cambridge, Cambridge CB2 3EA, United Kingdom

[3] Present address: School of Biosciences, University of Birmingham, Birmingham, United Kingdom

[4] Present address: Walter and Eliza Hall Institute of Medical Research, 1G Royal Parade, Parkville 3052, Australia

[5] Present address: Radachowka 37, 05-340 Kolbiel, Poland

[6] Corresponding authors:

Matthias Benoit: matthias.benoit@slcu.cam.ac.uk

Jerzy Paszkowski: jurek@paszkowski.com

Contact Information

Matthias Benoit: matthias.benoit@slcu.cam.ac.uk

Hajk-Georg Drost: hajk-georg.drost@slcu.cam.ac.uk

Marco Catoni: m.catoni@bham.ac.uk

Quentin Gouil: gouil.q@wehi.edu.au

Sara Lopez-Gomollon: sl750@cam.ac.uk

David Baulcombe: dcb40@cam.ac.uk

Jerzy Paszkowski: jurek@paszkowski.com

Running Title

Environmental and epigenetic control of *Rider* retrotransposons

Keywords

Tomato; LTR retrotransposon; drought stress; abscisic acid; small RNAs; DNA methylation

ABSTRACT

Transposable elements in crop plants are the powerful drivers of phenotypic variation that has been selected during domestication and breeding programs. In tomato, transpositions of the LTR (long terminal repeat) retrotransposon family *Rider* have contributed to various phenotypes of agronomical interest, such as fruit shape and colour. However, the mechanisms regulating *Rider* activity are largely unknown. We have developed a bioinformatics pipeline for the functional annotation of retrotransposons containing LTRs and defined all full-length *Rider* elements in the tomato genome. Subsequently, we showed that accumulation of *Rider* transcripts and transposition intermediates in the form of extrachromosomal DNA is triggered by drought stress and relies on abscisic acid signalling. We provide evidence that residual activity of *Rider* is controlled by epigenetic mechanisms involving siRNAs and the RNA-dependent DNA methylation pathway. Finally, we demonstrate the broad distribution of *Rider-like* elements in other plant species, including crops. Thus our work identifies *Rider* as an environment-responsive element and a potential source of genetic and epigenetic variation in plants.

INTRODUCTION

Transposable elements (TEs) replicate and move within host genomes. Based on their mechanisms of transposition, TEs are either DNA transposons that use a cut-and-paste mechanism or retrotransposons that transpose through an RNA intermediate via a copy-and-paste mechanism [1]. TEs make up a significant part of eukaryotic chromosomes and are a major source of genetic instability that, when active, can induce deleterious mutations. Various mechanisms have evolved that protect plant genomes, including the suppression of TE transcription by epigenetic silencing that restricts TE movement and accumulation [2–5].

Chromosomal copies of transcriptionally silenced TEs are typically hypermethylated at cytosine residues and are associated with nucleosomes containing histone H3 di-methylated at lysine 9 (H3K9me2). In addition, they are targeted by 24-nt small interfering RNAs (24-nt siRNAs) that guide RNA-dependent DNA methylation (RdDM), forming a self-reinforcing silencing loop [6–8]. Interference with these mechanisms can result in the activation of transposons. For example, loss of DNA METHYLTRANSFERASE 1 (MET1), the main methyltransferase maintaining methylation of cytosines preceding guanines (CGs), results in the activation of various TE families in Arabidopsis [9–11] and in rice [12]. Mutation of CHROMOMETHYLASE 3 (CMT3), mediating DNA methylation outside CGs, triggers the mobilization of several TE families, including *CACTA* elements in *Arabidopsis* [10] and *Tos17* and *Tos19* in rice [13]. Interference with the activity of the chromatin remodelling factor DECREASE IN DNA METHYLATION 1 (DDM1), as well as various components of the RdDM pathway, leads to the activation of specific subsets of TEs in Arabidopsis. These include DNA elements *CACTA* and *MULE*, as well as retrotransposons *ATGP3*, *COPIA13*, *COPIA21*, *VANDAL21*, *EVADÉ* and *DODGER* [14–17]. Similarly, loss of *OsDDM1* genes in rice results in the transcriptional activation of TE-derived sequences [18].

In addition to interference with epigenetic silencing, TE activation can also be triggered by environmental stresses. In her pioneering studies, Barbara McClintock denoted TEs as “controlling elements”, thus suggesting that they are activated by genomic stresses and are able to regulate the

activities of genes [19, 20]. In the meantime, a plethora of stress-induced TEs have been described, including retrotransposons. For example, the biotic stress-responsive *Tnt1* and *Tto1* families in tobacco [21,22], the cold-responsive *Tcs* family in citrus [23], the virus-induced *Bs1* retrotransposon in maize [24], the heat-responsive retrotransposons *Go-on* in rice [25], and *ONSEN* in Arabidopsis [26,27]. While heat-stress is sufficient to trigger *ONSEN* transcription and the formation of extrachromosomal DNA (ecDNA), transposition was observed only after the loss of siRNAs, suggesting that the combination of impaired epigenetic control and environmental stress is a prerequisite for *ONSEN* transposition [28]. Interestingly, retrotransposition occurs during flower development, which fuels the diversification of *ONSEN* insertion patterns in the progenies of plants permitting *ONSEN* movement [29].

The availability of high-quality genomic sequences revealed that LTR (Long Terminal Repeat) retrotransposons make up a significant proportion of plant chromosomes, from approximately 10% in Arabidopsis, 25% in rice, 42% in soybean, and up to 75% in maize [30]. In tomato (*Solanum lycopersicum*), a model crop plant for research on fruit development, LTR retrotransposons make up about 60% of the genome [31]. Despite the abundance of retrotransposons in the tomato genome, only a limited number of studies have linked TE activities causally to phenotypic alterations. Remarkably, the most striking examples described so far involve the retrotransposon family *Rider*. For example, fruit shape variation is based on copy number variation of the *SUN* gene, which underwent *Rider*-mediated trans-duplication from chromosome 10 to chromosome 7. The new insertion of the *SUN* gene into chromosome 7 in the variety “Sun1642” results in its overexpression and consequently in the elongated tomato fruits that were subsequently selected by breeders [32,33]. The *Rider* element generated an additional *SUN* locus on chromosome 7 that encompassed more than 20 kb of the ancestral *SUN* locus present on chromosome 10 [32]. This large “hybrid” retroelement landed in the fruit-expressed gene *DEFL1*, resulting in high and fruit-specific expression of the *SUN* gene containing the retroelement [33]. The transposition event was estimated to have occurred

within the last 200-500 years, suggesting that duplication of the *SUN* gene occurred after tomato domestication [34].

Jointless pedicel is a further example of a *Rider*-induced tomato phenotype that has been selected during tomato breeding. This phenotypic alteration reduces fruit dropping and thus facilitates mechanical harvesting. Several independent jointless alleles were identified around 1960 [35–37]. One of them involves a new insertion of *Rider* into the first intron of the *SEPALLATA* MADS-Box gene, *Solyc12g038510,* that provides an alternative transcription start site and results in an early nonsense mutation [38]. Also, the ancestral yellow flesh mutation in tomato is due to *Rider*-mediated disruption of the *PSY1* gene, which encodes a fruit-specific phytoene synthase involved in carotenoid biosynthesis [39,40]. Similarly, the “potato leaf” mutation is due to a *Rider* insertion in the *C* locus controlling leaf complexity [41]. *Rider* retrotransposition is also the cause of the chlorotic tomato mutant *fer*, identified in the 1960s [42]. This phenotype has been linked to *Rider*-mediated disruption of the *FER* gene encoding a bHLH-transcription factor. *Rider* landed in the first exon of the gene [43,44]. Sequence analysis of the element revealed that the causative copy of *Rider* is identical to that involved in the *SUN* gene duplication [44].

The *Rider* family belongs to the *Copia* superfamily and is ubiquitous in the tomato genome [33,44]. Based on partial tomato genome sequences, the number of *Rider* copies was estimated to be approximately 2000 [33]. Previous DNA blots indicated that *Rider* is also present in wild tomato relatives but is absent from the genomes of potato, tobacco, and coffee, suggesting that amplification of *Rider* happened after the divergence of potato and tomato approximately 6.2 mya [44,45]. The presence of *Rider* in unrelated plant species has also been suggested [46]. However, incomplete sub-optimal sampling and the low quality of genomic sequence assemblies has hindered a comprehensive survey of *Rider* elements within the plant kingdom.

Considering that the *Rider* family is a major source of phenotypic variation in tomato, it is surprising that its members and their basic activities, as well as their responsiveness and the possible triggers of environmental super-activation, which explain the evolutionary success of this family, remain

largely unknown. Contrary to the majority of TEs characterized to date, previous analyses revealed that *Rider* is constitutively transcribed and produces full-length transcripts in tomato [33], but the stimulatory conditions promoting reverse transcription of *Rider* transcripts that results in accumulation as extrachromosomal DNA are unknown.

To fill these gaps, we provide here a refined annotation of full-length *Rider* elements in tomato using the most recent genome release (SL3.0). We reveal environmental conditions facilitating *Rider* activation and show that *Rider* transcription is enhanced by dehydration stress mediated by abscisic acid (ABA) signalling, which also triggers accumulation of extrachromosomal DNA. Moreover, we provide evidence that RdDM controls *Rider* activity through siRNA production and partially through DNA methylation. Finally, we have performed a comprehensive cross-species comparison of full-length *Rider* elements in 110 plant genomes, including diverse tomato relatives and major crop plants, in order to characterise species-specific *Rider* features in the plant kingdom. Together, our findings suggest that *Rider* is a drought stress-induced retrotransposon ubiquitous in diverse plant species that may have contributed to phenotypic variation through the generation of genetic and epigenetic alterations induced by historical drought periods.

METHODS

Plant material and growth conditions

Tomato plants were grown under standard greenhouse conditions (16 h at 25°C with supplemental lighting of 88 w/m^2 and 8 h at 15°C without). *flacca* (*flc*), *notabilis* (*not*), and *sitiens* (*sit*) seeds were obtained from Andrew Thompson, Cranfield University; the *slnrpd1* and *slnrpe1* plants were described before [47]. For aseptic growth, seeds of *Solanum lycopersicum* cv. Ailsa Craig were surface-sterilized in 20% bleach for 10 min, rinsed three times with sterile H_2O, germinated and grown on half-strength MS media (16 h light and 8 h dark at 24°C).

Stress treatments

For dehydration stress, two-week-old greenhouse-grown plants were subjected to water deprivation for two weeks. For NaCl and mannitol treatments, tomato seedlings were grown aseptically for two weeks prior to transfer into half-strength MS solution containing 100, 200 or 300 nM NaCl or mannitol (Sigma) for 24 h. For abscisic acid (ABA) treatments, tomato seedlings were grown aseptically for two weeks prior to transfer into half-strength MS solution containing 0.5, 5, 10 or 100 µM ABA (Sigma) for 24 h. For 5-azacytidine treatments, tomato seedlings were germinated and grown aseptically on half-strength MS media containing 50 nM 5-azacytidine (Sigma) for two weeks. For cold stress experiments, two-week-old aseptically grown plants were transferred to 4°C for 24 h prior to sampling.

RNA extraction and quantitative RT-PCR analysis

Total RNA was extracted from 200 mg quick-frozen tissue using the TRI Reagent (Sigma) according to the manufacturer's instructions and resuspended in 50 µL H_2O. The RNA concentration was estimated using the Qubit Fluorometric Quantitation system (Thermo Fisher). cDNAs were synthesized using a SuperScript VILO cDNA Synthesis Kit (Invitrogen). Real-

time quantitative PCR was performed in the LightCycler 480 system (Roche) using primers listed in Table S1. LightCycler 480 SYBR Green I Master premix (Roche) was used to prepare the reaction mixture in a volume of 10 µL. Transcript levels were normalized to *SlACTIN* (*Solyc03g078400*). The results were analysed by the ΔΔCt method.

DNA extraction and copy number quantification

Tomato DNA was extracted using the Qiagen DNeasy Plant Mini Kit (Qiagen) following the manufacturer's instructions and resuspended in 30 µL H_2O. DNA concentration was estimated using the Qubit Fluorometric Quantitation system (Thermo Fisher). Quantitative PCR was performed in the LightCycler 480 system (Roche) using primers listed in Table S1. LightCycler 480 SYBR Green I Master premix (Roche) was used to prepare the reaction in a volume of 10 µL. DNA copy number was normalized to *SlACTIN* (*Solyc03g078400*). Results were analysed by the ΔΔCt method.

Extrachromosomal circular DNA detection

Extrachromosomal circular DNA amplification was derived from the previously published mobilome analysis [11]. In brief, extrachromosomal circular DNA was separated from chromosomal DNA using PlasmidSafe ATP-dependent DNase (EpiCentre) according to the manufacturer's instructions with the incubation at 37°C extended to 17 h. The PlasmidSafe exonuclease degrades linear DNA and thus safeguards circular DNA molecules. Circular DNA was precipitated overnight at -20°C in 0.1 v/v 3 M sodium acetate (pH 5.2), 2.5 v/v EtOH and 1 µL glycogen (Sigma). The pellet was resuspended in 20 µL H_2O. Inverse PCR reactions were carried out with 2 µL of DNA solution in a final volume of 20 µL using the GoTaq enzyme (Promega). The PCR conditions were as follows: denaturation at 95°C for 5 min, followed by 30 cycles at 95°C for 30 s, an annealing step for 30 s, an elongation step at 72°C for 60 s, and a final extension step at 72°C for 5 min. PCR products were separated in 1% agarose gels and developed by NuGenius (Syngene). Bands were extracted using the Qiagen Gel Extraction Kit and eluted in 30 µL H_2O. Purified

amplicons were subjected to Sanger sequencing. Primer sequences are listed in Table S1.

Phylogenetic analysis of de novo identified Rider elements

A phylogenetic tree was constructed from the nucleotide sequences of the 71 *Rider* elements using Geneious 9.1.8 (www.geneious.com) and built with the Tamura-Nei neighbor joining method. Pairwise alignment for the building distance matrix was obtained using a global alignment with free end gaps and a cost matrix of 51% similarity.

Distribution analysis

Genomic coordinates of each of the 71 *Rider* elements identified by *de novo* annotation using *LTRpred* (https://github.com/HajkD/LTRpred) have been used to establish their chromosomal locations. Coordinates for centromeres were provided before [31] and pericentromeric regions were defined by high levels of DNA methylation and H3K9me2.

Accession numbers

The Genbank accession number of the reference *Rider* nucleotide sequence identified in [44] is EU195798.2. We used *Solanum lycopersicum* bisulfite and small RNA sequencing data (SRP081115) generated in [47].

Dating of insertion time

Insertion times of *Rider* elements were estimated using the method described in [44]. Degrees of divergence between LTRs of each individual element were determined using *LTRpred*. LTR divergence rates were then converted into dates using the average substitution rate of 6.96×10^{-9} substitutions per synonymous site per year for tomato [48].

Bisulfite sequencing analysis

We collected data from previously published BS-seq libraries of tomato mutants of RNA polymerase IV and V and controls [47]: *slnrpe1* (SRR4013319), *slnrpd1* (SRR4013316), wild type *CAS9* (SRR4013314) and not transformed wild type (SRR4013312). The raw reads were analysed using our previously established pipeline [49] and aligned to the *Solanum lycopersicum* reference version SL3.0 (www.solgenomics.net/organism/Solanum_lycopersicum/genome). The chloroplast sequence (NC_007898) was used to estimate the bisulfite conversion (on average above 99%). The R package DMRcaller [50] was used to summarize the level of DNA methylation in the three cytosine contexts for each *Rider* copy.

Small RNA sequencing analysis

Tomato siRNA libraries were obtained from [47] and analysed using the same analysis pipeline to align reads to the tomato genome version SL3.0. Briefly, the reads were trimmed with Trim Galore! (www.bioinformatics.babraham.ac.uk/projects/trim_galore) and mapped using the ShortStack software v3.6 [51]. The siRNA counts on the loci overlapping *Rider* copies were calculated with R and the package Genomic Ranges.

Genome sequence data

Computationally reproducible analysis and annotation scripts for the following sections can be found at http://github.com/HajkD/RIDER.

Genomic data retrieval

We retrieved genome assemblies for 110 plant species (Table S2) from NCBI RefSeq [52] using the *meta.retrieval* function from the R package *biomartr* [53]. For *Solanum lycopersicum*, we retrieved the most recent genome assembly version SL3.0 from the *Sol Genomics Network* *ftp://ftp.solgenomics.net/tomato_genome/assembly/build_3.00/S_lycopersicum_chromosomes.3.00.fa* [54].

Functional *de novo* annotation of LTR retrotransposons in *Solanaceae* genomes

Functional *de novo* annotations of LTR retrotransposons for seventeen genomes from the *Asterids, Rosids,* and *monocot* clades (*Asterids*: *Capsicum annuum*, *C. baccatum MLFT02_5*, *C. chinense MCIT02_5*, *Coffea canephora*, *Petunia axillaris*, *Phytophthora inflata*, *Solanum arcanum*, *S. habrochaites*, *S. lycopersicum*, *S. melongena*, *S. pennellii*, *S. pimpinellifolium*, *S. tuberosum*; *Rosids*: *Arabidopsis thaliana*, *Vitis vinifera*, and *Cucumis melo*; *Monocots*: *Oryza sativa*) were generated using the *LTRpred.meta* function from the *LTRpred* annotation pipeline (https://github.com/HajkD/LTRpred; also used in [25]). To retrieve a consistent and comparable set of functional annotations for all genomes, we consistently applied the following *LTRpred* parameter configurations to all *Solanaceae* genomes: minlenltr = 100, maxlenltr = 5000, mindistltr = 4000, maxdisltr = 30000, mintsd = 3, maxtsd = 20, vic = 80, overlaps = “no”, xdrop = 7, motifmis = 1, pbsradius = 60, pbsalilen = c(8,40), pbsoffset = c(0,10), quality.filter = TRUE, n.orf = 0. The plant-specific tRNAs used to screen for primer binding sites (PBS) were retrieved from GtRNAdb [55] and plant RNA [56] and combined in a custom *fasta* file. The hidden Markov model files for gag and pol protein conservation screening were retrieved from Pfam [57] using the protein domains RdRP_1 (PF00680), RdRP_2 (PF00978), RdRP_3 (PF00998), RdRP_4 (PF02123), RVT_1 (PF00078), RVT_2 (PF07727), Integrase DNA binding domain (PF00552), Integrase zinc binding domain (PF02022), Retrotrans_gag (PF03732), RNase H (PF00075), and Integrase core domain (PF00665).

Sequence clustering of functional LTR retrotransposons from 17 genomes

We combined the *de novo* annotated LTR retrotransposons of the 17 species mentioned in the previous section in a large fasta file and used the cluster program *VSEARCH* [58] with parameter configurations: *vsearch --cluster_fast --qmask none –id 0.85 --clusterout_sort --clusterout_id --strand both --*

blast6out ---sizeout to cluster LTR retrotransposons by nucleotide sequence homology (global sequence alignments). Next, we retrieved the 85% sequence homology clusters from the *VSEARCH* output and screened for clusters containing *Rider* sequences. This procedure enabled us to detect high sequence homology (>85%) sequences of *Rider* across diverse species.

Nucleotide BLAST search of *Rider* against 110 plant genomes

To determine the distribution of *Rider* related sequences across the plant kingdom, we performed BLASTN [59] searches of *Rider* (= query sequence) using the function *blast_genomes* from the R package *metablastr* (https://github.com/HajkD/metablastr) against 110 plant genomes (Table S2) and the parameter configuration: *blastn -eval 1E-5 -max_target_seqs 5000*. As a result, we retrieved a BLAST hit table containing 11,748,202 BLAST hits. Next, we filtered for hits that contained at least 50% sequence coverage (= sequence homology) and throughout at least 50% sequence length homology to the reference *Rider* sequence. This procedure reduced the initial 11,748,202 BLAST hits to 57,845 hits, which we further refer to as *Rider-like* elements. These 57,845 *Rider-like* elements are distributed across 21 species with various abundance frequencies. In a second step, we performed an analogous BLASTN search using only the 5' LTR sequence of *Rider* to determine the distribution of *Rider-like* LTR across the plant kingdom. Using the same BLASTN search strategy described above, we retrieved 9,431 hits. After filtering for hits that contained at least 50% percent sequence coverage (= sequence homology) and at least 50% sequence length homology to the reference *Rider* LTR sequence, we obtained 2,342 BLAST hits distributed across five species.

Motif enrichment analysis

We tested the enrichment of *cis*-regulatory elements (CREs) in *Rider* compared to randomly sampled sequence loci from the same genome using the following procedure: first we sampled 1000 DNA sequences with the same length as the reference *Rider* sequence from 1000 randomly sampled loci in

the tomato reference genome. When sampling, we also considered the strand direction of the reference *Rider* sequence. Whenever a *Rider* sequence was annotated in the plus direction, we also sampled the corresponding set of random sequences in the plus direction of the respective randomly drawn locus. In contrast, when a *Rider* sequence was annotated in the minus direction, we also sampled the corresponding set of random sequences in the minus direction. Second, we counted CRE occurrences for each *Rider* sequence independently and for a set of different CREs. Next, we counted the number of the same CRE occurrences for each random sequence independently to assess how often these CREs were found in random sequences. We then constructed a 2x2 contingency table containing the respective motif count data of CRE observations in true *Rider* sequences *versus* counts in random sequences. We performed a Fisher's exact test for count data to assess the statistical significance of enrichment between the motif count data retrieved from *Rider* sequences and the motif count data retrieved from random sequences. The resulting *P*-values are shown in Tables S3 and S4 and the computationally reproducible scripts to perform the motif count analysis can be found at https://github.com/HajkD/RIDER.

Calculation of N50 metric

To assess the genome quality of *Solanaceae* species, we calculated the N50 metric for the genome assemblies of *Solanum lycopersicum, S. pimpinellifolium, S. arcanum, S. pennellii, S. habrochaites*, and *S. tuberosum* using the following procedure. First, we imported the scaffolds or chromosomes of each respective genome assembly using the R function *read_genome()* from the *biomartr* package. Next, for each species individually we determined the sequence length for each scaffold or chromosome and sorted them according to length in descending order. The N50 value in Mbp was then calculated in R as follows: *N50 <- len.sorted[cumsum(len.sorted) >= sum(len.sorted)*0.5][1] / 1000000*, where the variable *len.sorted* denotes the vector storing the ordered scaffold or chromosome lengths of a genome assembly.

RESULTS

Family structure of *Rider* retrotransposons in tomato

We used the most recent SL3.0 tomato genome release for *de novo* annotation of *Rider* elements. First, we retrieved full-length, potentially autonomous retrotransposons using our functional annotation pipeline (*LTRpred*, see Materials and Methods). We detected a set of 5844 potentially intact LTR retrotransposons (Table S5). Homology search among these elements identified 71 elements that share >85% similarity with the reference *Rider* sequence [44] and thus belong to the *Rider* family. We then determined the distribution of these *Rider* elements along the tomato chromosomes (Figure 1A) and also estimated their age based on sequence divergence between 5' and 3' LTRs (Figure 1A). We classified these elements into three categories according to their LTR similarity: 80-95%, 95-98% and 98-100% (Figure S1A). While the first category contains relatively old copies (last transposition between 10.5 and 3.5 mya), the 95-98% class represents *Rider* elements that moved between 3.5 and 1.4 mya, and the 98-100% category includes the youngest *Rider* copies that transposed within the last 1.4 my (Figure S1A). Out of 71 *Rider* family members, 14 were found in euchromatic chromosome arms (14/71 or 19.7%) and 57 in heterochromatic regions (80.3%) (Table 1). In accordance with previous observations based on partial genomic sequences [33], young *Rider* elements of the 98-100% class are more likely to reside in the proximity of genes, with 50% within 2 kb of a gene. This was the case for only 37.5% of old *Rider* members (85-95% class) (Table 2). Such a distribution is consistent with the preferential presence of young elements within euchromatic chromosome arms (50%, 5/10) compared to old *Rider* elements (9.4%, 3/32) (Table 2 and Figure S1B). The phylogenetic distance between individual elements is moderately correlated to the age of each element (Figure 1B) (Table S6), suggesting that the recent amplification of *Rider* was due to the activity of young intact elements.

448 **_Rider_ is a drought- and ABA-responsive retrotransposon**

449

450 To better understand the activation triggers and, thus, the mechanisms
451 involved in the accumulation of *Rider* elements in the tomato genome, we
452 examined possible environmental stresses and host regulatory mechanisms
453 influencing their activity. Transcription of an LTR retroelement initiates in its 5'
454 LTR and is regulated by an adjacent promoter region that usually contains *cis*-
455 regulatory elements (CREs) (reviewed in [60]). Therefore, we aligned the
456 sequence of the *Rider* promoter region against sequences stored in the
457 PLACE database (www.dna.affrc.go.jp/PLACE/) containing known CREs and
458 identified several dehydration-responsive elements (DREs) and sequence
459 motifs linked to ABA signalling (Figure 2A). First, we tested whether these
460 CREs were significantly enriched in the LTR promoter sequences of the 71 *de*
461 *novo* annotated *Rider* elements. Comparison of *Rider* LTRs to a set of
462 randomly selected genomic sequences of the same length revealed
463 significant enrichment of several CREs in *Rider* LTRs (Fisher's exact test
464 $P<0.001$) (Table S3). It is known, for example, that the CGCG sequence motif
465 at position 89-94 (Figure 2A) is recognized by transcriptional regulators
466 binding calmodulin. These are products of signal-responsive genes activated
467 by various environmental stresses and phytohormones such as ABA [61]. We
468 also detected two MYB recognition sequence motifs (CTGTTG at position
469 176-181 bp, and CTGTTA at position 204-209 bp) (Figure 2A). MYB
470 recognition sequences are usually enriched in the promoters of genes with
471 transcriptional activation during water stress, elevated salinity, and ABA
472 treatments [62,63]. In addition, an ABA-responsive element-like (ABRE-like)
473 was found at position 332-337 bp in the R region of *Rider*'s LTR, along with a
474 coupling element (CE3) located at position 357-372 bp (Figure 2A). The co-
475 occurrence of ABRE-like and CE3 has often been found in ABA-responsive
476 genes [64,65].

477 The simultaneous presence of these five CREs in promoters of *Rider*
478 elements suggests that *Rider* transcription may be induced by environmental
479 stresses such as dehydration and salinity that involves ABA mediated
480 signalling. To test whether *Rider* transcription is stimulated by drought stress,
481 glasshouse-grown tomato plants were subjected to water deprivation and

levels of *Rider* transcripts quantified by RT-qPCR (Figure 2B). When compared to control plants, we observed a 4.4-fold increase in *Rider* transcript abundance in plants subjected to drought stress. Thus, *Rider* transcription appears to be stimulated by drought.

To further test this finding, we re-measured levels of *Rider* transcripts in different experimental setups. *In vitro* culture conditions with increasing levels of osmotic stress were used to mimic increasing drought severity (Figure 2C). Transcript levels of *Rider* increased in a dose-dependent fashion with increasing mannitol concentration, corroborating results obtained during direct drought stress in greenhouse conditions. Interestingly, tomato seedlings treated with NaCl also exhibited increased levels of *Rider* transcripts (Figure 2C).

ABA is a versatile phytohormone involved in plant development and abiotic stress responses, including drought stress [66]. Therefore, we asked whether *Rider* transcriptional drought-responsiveness is mediated by ABA and whether increased ABA can directly stimulate *Rider* transcript accumulation. To answer the first question, we exploited tomato mutants defective in ABA biosynthesis. The lines *flacca* (*flc*), *notabilis* (*not*) and *sitiens* (*sit*) have mutations in genes encoding a sulphurylase [67], a 9-cis-epoxy-carotenoid dioxygenase (*SlNCED1*) [68,69], and an aldehyde oxidase [70], respectively. Both *flc* and *sit* are impaired in the conversion of ABA-aldehyde to ABA [67,70], while *not* is unable to catalyse the cleavage of 9-cis-violaxanthin and/or 9-cis-neoxanthin to xanthoxin, an ABA precursor [69]. Glasshouse-grown *flc*, *not* and *sit* mutants and control wild-type plants were subjected to water deprivation treatment and *Rider* transcript levels quantified by RT-qPCR (Figure 2D). *Rider* transcript levels were reduced in *flc*, *not* and *sit* by 43%, 26% and 56%, respectively.

To examine whether ABA stimulates accumulation of *Rider* transcripts, tomato seedlings were transferred to media supplemented with increasing concentrations of ABA (Figure 2E). The levels of *Rider* transcripts increased in a dose-dependent manner with increasing ABA concentrations. This suggests that ABA is not only involved in signalling that results in hyper-activation of *Rider* transcription during drought, but it also directly promotes the accumulation of *Rider* transcripts. The effectiveness of the treatments was

516 verified by assaying expression of the stress- and ABA-responsive gene
517 *SlASR1* (Figure S2A-F).
518 Identification in the U3 region of *Rider* LTRs of a binding domain for C-
519 repeat binding factors (CBF), which are regulators of the cold-induced
520 transcriptional cascade [64,71], led us to test *Rider* activation by cold stress.
521 However, *Rider* transcription was not affected by cold treatment, leaving
522 drought and salinity as the predominant environmental stresses identified so
523 far that stimulate accumulation of *Rider* transcripts (Figure S2G).
524
525 **RdDM regulates levels of *Rider* transcripts**
526
527 The suppression of transposon-derived transcription by epigenetic
528 mechanisms, which typically include DNA methylation, maintains genome
529 integrity [2,3,5]. We asked whether *Rider* transcription is also restricted by
530 DNA methylation. Tomato seedlings were grown on media supplemented with
531 5-azacytidine, an inhibitor of DNA methyltransferases. *Rider* transcript steady-
532 state levels increased in plants treated with 5-azacytidine compared to
533 controls (Figure 3A). Comparison of *Rider* transcript accumulation in 5-
534 azacytidine-treated and ABA-treated plants revealed similar levels of
535 transcripts and the levels were similar when the treatments were applied
536 together (P <0.05; Figure 3A).
537 To further examine the role of DNA methylation in controlling *Rider*
538 transcription, we took advantage of tomato mutants defective in crucial
539 components of the RdDM pathway, namely SlNRPD1 and SlNRPE1, the
540 major subunits of RNA Pol IV and Pol V, respectively. These mutants exhibit
541 reduced cytosine methylation at CHG and CHH sites (in which H is any base
542 other than G) residing mostly at the chromosome arms, with *slnrpd1* showing
543 a dramatic, genome-wide loss of 24-nt siRNAs [47]. To evaluate the role of
544 RdDM in *Rider* transcript accumulation, we first assessed the consequences
545 of impaired RdDM on siRNA populations at full-length *Rider* elements.
546 Deficiency in SlNRPD1 resulted in a complete loss of 24-nt siRNAs that target
547 *Rider* elements (Figure 3B). This loss was accompanied by a dramatic
548 increase (approximately 80-fold) in 21-22-nt siRNAs at *Rider* loci (Figure 3B).
549 In contrast, the mutation in SlNRPE1 triggered increases in both 21-22-nt and

24-nt siRNAs targeting *Rider* elements (Figure 3B). We then asked whether altered distribution of these siRNA classes is related to the age of the *Rider* elements and/or their chromosomal position, and thus local chromatin properties. Compilation of the genomic positions and siRNA data suggests a preferential increase in levels of 21-22-nt siRNAs in *slnrpd1*, and to a lesser extent in *slnrpe1,* for young *Rider* elements (98-100 class) and *Rider* copies located in euchromatin (Figure S3A). In contrast, accumulation of 24-nt siRNAs was not related to any particular sub-class of elements or their chromosomal positions (Figure S3B). Subsequently, we examined whether loss of SlNRPD1 or SlNRPE1 was sufficient to increase levels of *Rider* transcripts and observed increased accumulation of *Rider* transcripts in both *slnrpd1* and *slnrpe1* compared to WT (Figure 3C).

We assessed whether this increase in *Rider* transcript levels is linked to changes in DNA methylation levels in *Rider* elements of RdDM mutants. There was no significant change in global DNA methylation in the three sequence contexts in the 71 *de novo* annotated *Rider* elements (Figure S3C), despite a tendency for young *Rider* elements to lose CHH in *slnrpd1* and *slnrpe1* (Figure S3D). Thus, the RdDM pathway affects the levels of *Rider* transcripts but there was no direct link to DNA methylation levels.

Extrachromosomal circular DNA of *Rider* accumulates during drought stress and in *slnrpd1* and *slnrpe1* mutants

The life cycle of LTR retrotransposons starts with transcription of the element, then the synthesis and maturation of accessory proteins including reverse transcriptase and integrase, reverse transcription, and the production of extrachromosomal linear (ecl) DNA that integrates into a new genomic location [72]. In addition, eclDNA can be a target of DNA repair and can be circularised by a non-homologous end-joining mechanism or homologous recombination between LTRs, resulting in extrachromosomal circular DNA (eccDNA) [73–76]. We searched for eccDNA to evaluate the consequences of increased *Rider* transcript accumulation due to drought stress or an impaired RdDM pathway on subsequent steps of the transposition cycle. After exonuclease-mediated elimination of linear dsDNA and circular ssDNA, *Rider*

584 eccDNA was amplified by sequence-specific inverse PCR (Figure 4A). *Rider*
585 eccDNA was absent in plants grown in control conditions but was detected in
586 plants subjected to drought stress (Figure 4A). Sanger sequencing of the
587 inverse PCR products showed that the amplified eccDNA probably originates
588 from the *Rider_08_3* copy, which has 98.2 % sequence homology of the 5'
589 and 3' LTR sequences (Figure S4A). Residual sequence divergence may be
590 due to genotypic differences between the reference genomic sequence and
591 the genome of our experimental material. Analysis of CREs in the LTR of the
592 eccDNA revealed the presence of all elements identified previously with the
593 exception of a single nucleotide mutation located in the *CGCGBOXAT* box
594 (Figure S4A). This suggests that while this CRE is not required for production
595 of *Rider* eccDNA upon drought stress, presence of all other CREs including
596 the two *MYBCORE* elements is likely to be necessary for its activation.
597 Examination by quantitative PCR of the accumulation of *Rider* DNA,
598 which included extrachromosomal and integrated copies, in drought-stressed
599 plants also revealed an increase in *Rider* copy number (Figure 4B).
600 Importantly, *Rider* eccDNA was not detected in *sit* mutants subjected to
601 drought stress (Figure 4A), suggesting that induced transcription of *Rider* by
602 drought stress triggers production of extrachromosomal DNA and this
603 response requires ABA biosynthesis.
604 We also examined the accumulation of *Rider* eccDNA in plants
605 impaired in RdDM. Interestingly, *Rider* eccDNA was detected in *slnrpd1* and
606 *slnrpe1* (Figure 4C) and increase in *Rider* DNA copy number was confirmed
607 by qPCR (Figure 4D). The eccDNA forms differed between the mutants
608 (Figure 4C). Sequencing of *Rider* eccDNA in *slnrpd1* showed a sequence
609 identical to the *Rider* eccDNA of wild-type plants subjected to drought stress.
610 Thus the *Rider_08_3* copy is probably the main contributor to eccDNA in
611 drought and in *slnrpd1*. In contrast, eccDNA recovered from *slnrpe1* had a
612 shorter LTR (287 bp) and the highest sequence similarity with *Rider_07_2*
613 (89.2 %) (Figure S4B). Shortening of the LTR in this particular element is
614 associated with the loss of the upstream *MYBCORE* as well as the
615 *CGCGBOXAT* elements (Figure S4B). This suggests that in the absence of
616 SlNRPE1, presence of these CREs is facultative for eccDNA production
617 originating from this copy. In contrast, the absence of eccDNA copies derived

618 from this element upon dehydration suggests that both *MYBCORE* elements
619 are required for effective *Rider* activation upon drought stress.
620 We then asked whether DNA methylation and siRNA distribution at
621 these particular *Rider* copies had changed in the mutants. DNA methylation at
622 CHH sites was drastically reduced at *Rider_08_3* in *slnrpd1* (Figure 4E and
623 Figure S4C) together with a complete loss of 24-nt siRNAs at this locus
624 (Figure 4F and Figure S4D) but DNA methylation at *Rider_07_2* was not
625 affected, despite the deficiency of SlNRPD1 or SlNRPE1 (Figure 4E and
626 Figure S4C). Levels of 21-22-nt siRNAs in both mutants and 24-nt siRNA in
627 *slnrpe1* were increased (Figure 4F and Figure S4E). Altogether, this suggests
628 that different components of the RdDM pathway differ in their effects on the
629 activity of individual members of the *Rider* retrotransposon family.
630
631 **_Rider_ families in other plant species**
632
633 To examine the distribution of *Rider* retrotransposons in other plant
634 species, we searched for *Rider*-related sequences across the genomes of
635 further *Solanaceae* species, including wild tomatoes, potato (*Solanum*
636 *tuberosum*), and pepper (*Capsicum annuum*). We used the *Rider* reference
637 sequence [44] as the query against genome sequences of *Solanum arcanum*,
638 *S. habrochaites*, *S. lycopersicum*, *S. pennellii*, *S. pimpinellifolium*, *S.*
639 *tuberosum,* and *Capsicum annuum* (genome versions are listed in Materials
640 and Methods). Two BLAST searches were performed, one using the entire
641 *Rider* sequence as the query and the other using only the *Rider* LTR.
642 Consistent with previous reports, *Rider-like* elements are present in wild
643 relatives of tomato such as *S. arcanum*, *S. pennellii* and *S. habrochaites;*
644 however, the homology levels and their lengths vary significantly between
645 species (Figure 5A). While *S. arcanum* and *S. habrochaites* exhibit high peak
646 densities at 55% and 61% homology, respectively, *S. pennellii* show a high
647 peak density at 98% over the entire *Rider* reference sequence (Figure 5A).
648 This suggests that the *S. arcanum* and *S. habrochaites* genomes harbour
649 mostly *Rider-like* elements with relatively low sequence similarity, while *S.*
650 *pennellii* retains full-length *Rider* elements.

651 To better visualize this situation, we aligned the BLAST hits to the
652 reference *Rider* copy (Figure 5B). This confirmed that *Rider* elements in *S.*
653 *pennellii* are indeed mostly full-length *Rider* homologs showing high density of
654 hits throughout their lengths, while BLAST hits in the *S. arcanum* and *S.*
655 *habrochaites* genomes showed only partial matches over the 4867 bp of the
656 reference *Rider* sequence (Figure 5B). Unexpectedly, this approach failed to
657 detect either full-length or truncated *Rider* homologs in the close relative *of*
658 tomato, *S. pimpinellifolium*. Extension of the same approaches to the
659 genomes of the evolutionary more distant *S. tuberosum* and *Capsicum*
660 *annuum* failed to detect substantial *Rider* homologs (Figure 5A-B), confirming
661 the absence of *Rider* in the potato and pepper genomes [44]. As a control, we
662 also analysed *Arabidopsis thaliana*, since previous studies reported the
663 presence of *Rider* homologs in this model plant [44]. Using the BLAST
664 approach above, we repeated the results provided in [44] and found BLAST
665 hits of high sequence homology to internal sequences of *Rider* in the
666 *Arabidopsis thaliana* genome. However, we did not detect sequence
667 homologies to *Rider* LTRs (Figure 5C-D). Motivated by this finding and the
668 possibility that *Rider* homologs in other species may have highly divergent
669 LTRs, we screened for *Rider* LTRs that would have been missed in the
670 analysis shown in Figure 5A-B due to the use of the full-length sequence of
671 *Rider* as the query. Using the *Rider* LTR as a query revealed that *S. pennellii,*
672 *S. arcanum* and *S. habrochaites* retain intact *Rider* LTR homologs, but *S.*
673 *pimpinellifolium* exhibits a high BLAST hit density exclusively at approximately
674 60% homology. This suggests strong divergence of *Rider* LTRs in this species
675 (Figure 5C-D). Overall, the results indicate intact *Rider* homologs in some
676 *Solanaceae* species, whereas sequence similarities to *Rider* occur only within
677 the coding area of the retrotransposons in more distant plants such as
678 *Arabidopsis thaliana.* Therefore, LTRs, which include the *cis*-regulatory
679 elements conferring stress-responsiveness, diverge markedly between
680 species.
681 To address the specificity of this divergence in *Solanaceae* species, we
682 examined whether the CREs enriched in *S. lycopersicum* (Figure 2A) are
683 present in LTR sequences of the *Rider* elements in *S. pennellii, S. arcanum*,
684 *S. habrochaites* and *S. pimpinellifolium* (Figure 5C). While the LTRs identified

in *S. pennellii, S. arcanum* and *S. habrochaites* retained all five previously identified CREs, more distant LTRs showed shortening of the U3 region associated with loss of the CGCG box (Figure S5 and Table S4). This was observed already in *S. pimpinellifolium*, where all identified *Rider* LTRs lacked part of the U3 region containing the CGCG box (Supplementary Figure 5). Thus, *Rider* distribution and associated features differ even between closely related *Solanaceae* species, correlated with the occurrence of a truncated U3 region and family-wide loss of CREs.

Finally, to test the evolutionary conservation of *Rider* elements across the plant kingdom, we performed *Rider* BLAST searches against all 110 plant genomes available at the NCBI Reference Sequence (RefSeq) database (www.ncbi.nlm.nih.gov/refseq). Using the entire *Rider* sequence as the query to measure the abundance of *Rider* homologs throughout these genomes, we found *Rider* homologs in 14 diverse plant species (Figure S6). This suggests that *Rider* in tomato did not originate by horizontal transfer from Arabidopsis as initially suggested [44], but rather that *Rider* was already present in the last common ancestor of these plant species and persisted or was subsequently eradicated from the genomes. The limited conservation of *Rider* LTR sequences in the same 14 species, revealed using the LTR sequence as the query, suggests that *Rider* LTRs are rapidly evolving and that drought-responsive CREs may be restricted to *Solanaceae* (Figure S7).

DISCUSSION

High-resolution map of full-length Rider elements in the tomato genome

Comprehensive analysis of individual LTR retrotransposon families in complex plant genomes has been facilitated and become more accurate with the increasing availability of high-quality genome assemblies. Here, we took advantage of the most recent tomato genome release (SL3.0) to characterize with improved resolution the high-copy-number *Rider* retrotransposon family. Although *Rider* activity has been causally linked to the emergence of important agronomic phenotypes in tomato, the triggers of *Rider* have remained elusive. Despite the relatively low proportion (approximately 20%) of euchromatic chromosomal regions in the tomato genome [31]), our *de novo* functional annotation of full-length *Rider* elements revealed preferential compartmentalization of recent *Rider* insertions within euchromatin compared to aged insertions. Mapping analyses further revealed that recent rather than aged *Rider* transposition events are more likely to modify the close vicinity of genes. However, *Rider* copies inserted into heterochromatin have been passively maintained for longer periods. This differs significantly from other retrotransposon families in tomato such as *Tnt1*, *ToRTL1* and *T135,* which show initial, preferential insertions into heterochromatic regions [77]. *TARE1*, a high-copy-number *Copia-like* element, is present predominantly in pericentromeric heterochromatin [78]. Another high-copy-number retrotransposon, *Jinling*, is also enriched in heterochromatic regions, making up about 2.5% of the tomato nuclear genome [79]. The *Rider* propensity to insert into gene-rich areas mirrors the insertional preferences of the *ONSEN* family in Arabidopsis. Since new *ONSEN* insertions confer heat-responsiveness to neighbouring genes [28,29], it is tempting to speculate that genes in the vicinity of new *Rider* insertions may acquire, at least transiently, drought-responsiveness.

742 *Environmental and epigenetic regulation of Rider activity*

743

744 We found that *Rider* transcript levels are elevated during dehydration stress
745 mediated by ABA-dependent signalling. The activation of retrotransposons
746 upon environmental cues has been shown extensively to rely on the presence
747 of *cis*-regulatory elements within the retrotransposon LTRs [60]. The heat-
748 responsiveness of *ONSEN* in Arabidopsis [26,27,80], *Go-on* in rice [25], and
749 *Copia* in Drosophila [81] is conferred by the presence in their LTRs of
750 consensus sequences found in the promoters of heat-shock responsive
751 genes. Thus, the host's heat-stress signalling appears to induce
752 transcriptional activation of the transposon and promote transposition [80].
753 While *ONSEN* and *Go-on* are transcriptionally inert in the absence of a
754 triggering stress, transcripts of Drosophila *Copia* are found in control
755 conditions, resembling the regulatory situation in *Rider*. Due to relatively high
756 constitutive expression, increase in transcript levels of Drosophila *Copia*
757 following stress appears modest compared to *ONSEN* or *Go-on*, which are
758 virtually silent in control conditions [25–27,80]. Regulation of Drosophila *Copia*
759 mirrors that of *Rider*, where transcript levels during dehydration stress are
760 very high but the relative increase compared to control conditions is rather
761 modest.

762 The presence of MYB recognition sequences within *Rider* LTRs
763 suggests that MYB transcription factors participate in transcriptional activation
764 of *Rider* during dehydration. Multiple MYB subfamilies are involved in ABA-
765 dependent stress responses in tomato, but strong enrichment of the MYB
766 core element CTGTTA within *Rider* LTRs suggests involvement of R2R3-MYB
767 transcription factors, which are markedly amplified in *Solanaceae* [82].
768 Members of this MYB subfamily are involved in the ABA signalling-mediated
769 drought-stress response [83] and salt-stress signalling [84]. This possible
770 involvement of R2R3-MYBs in *Rider* is reminiscent of the transcriptional
771 activation of the tobacco retrotransposon *Tto1* by the R2R3-MYB, member
772 NtMYB2 [85].

773 In addition to environmental triggers, *Rider* transcript levels are
774 regulated by the RdDM pathway. Depletion of SlNRPD1 and SlNRPE1
775 increases *Rider* transcript abundance, resulting in production of

extrachromosomal circular DNA. Analysis of *Rider*-specific siRNA populations revealed that siRNA targeting of *Rider* elements is mostly independent of their genomic location and chromatin context. This is somewhat unexpected since RdDM activity in tomato seems to be restricted to gene-rich euchromatin and it was postulated that accessibility of RNA Pol IV to heterochromatin is hindered by the compact chromatin structure [47,86,87]. We found that virtually all *Rider* copies are RdDM targets, which potentially influences local epigenetic features. Loss of SlNRPD1 and SlNRPE1 leads to over-accumulation of 21-22-nt siRNAs at *Rider* copies, suggesting that inactivation of canonical RdDM pathway-dependent transcriptional gene silencing triggers the activity of the non-canonical RDR6 RdDM pathway at *Rider* [88–90].

It is noteworthy that, despite clear effects on *Rider* transcript accumulation and siRNA accumulation, loss of SlNRPD1 and SlNRPE1 is not manifested by drastic changes in DNA methylation levels of *Rider* at the family level. Only young euchromatic *Rider* elements marginally lose CHH methylation in the *slnrpd1* mutant, but this is modest compared to the general decrease in mCHH observed throughout the chromosome arms [47]. As expected, CHH methylation at heterochromatic *Rider* is not affected. This suggests that SlCMT2 is involved in maintenance of mCHH at heterochromatic *Rider* copies in the absence of SlNRPD1, as observed previously for pericentromeric heterochromatin [47]. In general, our observations suggest that epigenetic silencing of *Rider* retrotransposons is particularly robust and involves compensatory pathways.

We identified extrachromosomal circular DNA originating from the *Rider* copies *Rider_08_3* and *Rider_07_2* in *slnrpd1* and *slnrpe1*, respectively. In terms of DNA methylation and siRNA distribution at these two specific copies, loss of SlNRPD1 and SlNRPE1 brought different copy-specific outcomes. *Rider_08_3*, the main contributor to eccDNA in *slnrpd1,* displayed a reduction in CHH methylation that may contribute to increased transcription and the accumulation of eccDNA. In *Rider_07_2,* that provides a template for eccDNA in *slnrpe1*, there was no change in DNA methylation levels. Therefore, transcription and the production of eccDNA from this *Rider* copy is not regulated by DNA methylation. Consequently, eccDNA from *Rider_07_2* was not detected in *slnrpd1* despite drastic loss of CHH methylation.

Altogether, it appears that transcriptional control and reverse transcription of *Rider* copies occurs via multiple layers of regulation, possibly specific for individual *Rider* elements according to age, sequence or genomic location, that are targeted by parallel silencing pathways, including non-canonical RdDM [91,92].

Rider retrotransposons in other plant species

The presence of *Rider* in tomato relatives as well as in more distantly related plant species has been described previously [33,44,46]. However, the *de novo* identification of *Rider* elements in the sampling provided here shows the distribution of the *Rider* family within plant species to be more complex than initially suggested. Surprisingly, mining for sequences with high similarity, overlapping more than 85% of the entire reference sequence of *Rider*, detected no full-length *Rider* elements in *Solanum pimpinellifolium* but in all other wild tomato species tested. Furthermore, the significant accumulation of only partial *Rider* copies in *Solanum pimpinellifolium*, the closest relative of tomato, does not match the established phylogeny of the *Solanaceae*. The cause of these patterns is unresolved but two scenarios can be envisaged. First, the absence of full-length *Rider* elements may be due to the suboptimal quality of genome assembly that may exclude a significant proportion of highly repetitive sequences such as *Rider*. This is supported by the N50 values within the *Solanaceae*, where the quality of genome assemblies varies significantly between species, with *S. pimpinellifolium* showing the lowest (Table S7). An improved genome assembly would allow a refined analysis of *Rider* in this species. Alternatively, active *Rider* copies may have been lost in *S. pimpinellifolium* since the separation from the last common ancestor but not in the *S. lycopersicum* and *S. pennellii* lineages. The high-density of solo-LTRs and truncated elements in *S. pimpinellifolium* is in agreement with this hypothesis.

Comparing the sequences of *Rider* LTRs in the five tomato species, the unique occurrence of LTRs lacking most of the U3 region in *S. pimpinnellifolium* suggests that loss of important regulatory sequences has impeded maintenance of intact *Rider* elements. Interestingly, part of the U3

844 region missing in *S. pimpinellifolium* contains the CGCG box, which is
845 involved in response to environmental signals [61], as well as a short CpG-
846 island-like structure (position 52-155 bp on reference *Rider*). CpG islands are
847 usually enriched 5' of transcriptionally active genes in vertebrates [93] and
848 plants [94]. Despite the presence of truncated *Rider* LTRs, the occurrence of
849 intact, full-length LTRs in other wild tomato species indicates that *Rider* is still
850 potentially active in these genomes.
851 Altogether, our findings suggest that inter- and intra-species TE
852 distribution can be uncoupled and that the evolution of TE families in present
853 crop plants was more complex than initially anticipated. Finally, we have
854 opened interesting perspectives for harnessing transposon activities in crop
855 breeding. Potentially active TE families that react to environmental stimuli,
856 such as *Rider*, provide an unprecedented opportunity to generate genetic and
857 epigenetic variation from which desirable agronomical traits may emerge.
858 Notably, rewiring of gene expression networks regulating the drought-stress
859 responses of new *Rider* insertions is an interesting strategy to engineer
860 drought-resilient crops.
861

Acknowledgments

Funding

This work was supported by the European Research Council (EVOBREED, No. 322621) and the Gatsby Charitable Foundation (Fellowship AT3273/GLE).

Disclosure Declaration

The authors declare no competing interests.

Author contribution

MB and JP designed the study; MB performed experiments; MB, HGD and MC performed genomic data analyses; QG, SLG and DCB provided unpublished material and data; MB and JP wrote the paper with contributions from HGD and MC. All authors read and approved the final manuscript.

The authors thank all members of Dr. Paszkowski lab for fruitful discussions during the development of this project as well as the SLCU support staff.

REFERENCES

1. Lisch D (2013) How important are transposons for plant evolution? *Nat Rev Genet* **14**: 49–61.
2. Lisch D (2009) Epigenetic Regulation of Transposable Elements in Plants. *Annu Rev Plant Biol* **60**: 43–66.
3. Slotkin RK, Martienssen R (2007) Transposable elements and the epigenetic regulation of the genome. *Nat Rev Genet* **8**: 272–285.
4. Zhang H, Zhu J-K (2011) RNA-directed DNA methylation. *Curr Opin Plant Biol* **14**: 142–147.
5. Rigal M, Mathieu O (2011) A ‘mille-feuille’ of silencing: Epigenetic

control of transposable elements. *Biochim Biophys Acta - Gene Regul Mech* **1809**: 452–458.

6. Law JA, Jacobsen SE (2010) Establishing, maintaining and modifying DNA methylation patterns in plants and animals. *Nat Rev Genet* **11**: 204–220.
7. Matzke M, Kanno T, Huettel B, Daxinger L, Matzke AJM (2007) Targets of RNA-directed DNA methylation. *Curr Opin Plant Biol* **10**: 512–519.
8. Wendte JM, Pikaard CS (2017) The RNAs of RNA-directed DNA methylation. *Biochim Biophys Acta* **1860**: 140–148.
9. Mirouze M, Reinders J, Bucher E, Nishimura T, Schneeberger K, Ossowski S, Cao J, Weigel D, Paszkowski J, Mathieu O (2009) Selective epigenetic control of retrotransposition in Arabidopsis. *Nature* **461**: 1–5.
10. Kato M, Miura A, Bender J, Jacobsen SE, Kakutani T (2003) Role of CG and non-CG methylation in immobilization of transposons in Arabidopsis. *Curr Biol* **13**: 421–426.
11. Lanciano S, Carpentier MC, Llauro C, Jobet E, Robakowska-Hyzorek D, Lasserre E, Ghesquière A, Panaud O, Mirouze M (2017) Sequencing the extrachromosomal circular mobilome reveals retrotransposon activity in plants. *PLoS Genet* **13**: 1–20.
12. Hu L, Li N, Xu C, Zhong S, Lin X, Yang J, Zhou T, Yuliang A, Wu Y, Chen Y-R, et al. (2014) Mutation of a major CG methylase in rice causes genome-wide hypomethylation, dysregulated genome expression, and seedling lethality. *Proc Natl Acad Sci* **111**: 10642–10647.
13. Cheng C, Tarutani Y, Miyao A, Ito T, Yamazaki M, Sakai H, Fukai E, Hirochika H (2015) Loss of function mutations in the rice chromomethylase OsCMT3a cause a burst of transposition. *Plant J* **83**: 1069–1081.
14. Miura A, Yonebayashi S, Watanabe K, Toyama T, Shimada H, Kakutani T (2001) Mobilization of transposons by a mutation abolishing full DNA methylation in Arabidopsis. *Nature* **411**: 212–214.
15. Lippman Z, Gendrel A-V, Black M, Vaughn MW, Dedhia N, McCombie WR, Lavine K, Mittal V, May B, Kasschau KD, et al. (2004) Role of

transposable elements in heterochromatin and epigenetic control. *Nature* **430**: 471–476.

16. Tsukahara S, Kobayashi A, Kawabe A, Mathieu O, Miura A, Kakutani T (2009) Bursts of retrotransposition reproduced in Arabidopsis. *Nature* **461**: 423–426.
17. Griffiths J, Catoni M, Iwasaki M, Paszkowski J (2018) Sequence-Independent Identification of Active LTR Retrotransposons in Arabidopsis. *Mol Plant* **11**: 508–511.
18. Tan F, Zhou C, Zhou Q, Zhou S, Yang W, Zhao Y, Li G, Zhou D-X (2016) Analysis of Chromatin Regulators Reveals Specific Features of Rice DNA Methylation Pathways. *Plant Physiol* **171**: 2041–2054.
19. Chuong EB, Elde NC, Feschotte C (2017) Regulatory activities of transposable elements: from conflicts to benefits. *Nat Rev Genet* **18**: 71–86.
20. McClintock B (1951) Chromosome Organization and Genic Expression. *Cold Spring Harb Symp Quant Biol* **16**: 13–47.
21. Grandbastien MA (1998) Activation of plant retrotransposons under stress conditions. *Trends Plant Sci* **3**: 181–187.
22. Grandbastien MA, Audeon C, Bonnivard E, Casacuberta JM, Chalhoub B, Costa APP, Le QH, Melayah D, Petit M, Poncet C, et al. (2005) Stress activation and genomic impact of Tnt1 retrotransposons in Solanaceae. *Cytogenet Genome Res* **110**: 229–241.
23. Butelli E, Licciardello C, Zhang Y, Liu J, Mackay S, Bailey P, Reforgiato-Recupero G, Martin C (2012) Retrotransposons Control Fruit-Specific, Cold-Dependent Accumulation of Anthocyanins in Blood Oranges. *Plant Cell* **24**: 1242–1255.
24. Johns M a, Mottinger J, Freeling M (1985) A low copy number, copia-like transposon in maize. *EMBO J* **4**: 1093–1101.
25. Cho J, Benoit M, Catoni M, Drost H-G, Brestovitsky A, Oosterbeek M, Paszkowski J (2019) Sensitive detection of pre-integration intermediates of long terminal repeat retrotransposons in crop plants. *Nat. Plants* **5**: 26-33.
26. Tittel-Elmer M, Bucher E, Broger L, Mathieu O, Paszkowski J, Vaillant I (2010) Stress-Induced Activation of Heterochromatic Transcription.

PLoS Genet **6**: e1001175.

27. Pecinka A, Dinh HQ, Baubec T, Rosa M, Lettner N, Scheid OM (2010) Epigenetic Regulation of Repetitive Elements Is Attenuated by Prolonged Heat Stress in *Arabidopsis*. *Plant Cell* **22**: 3118–3129.
28. Ito H, Gaubert H, Bucher E, Mirouze M, Vaillant I, Paszkowski J (2011) An siRNA pathway prevents transgenerational retrotransposition in plants subjected to stress. *Nature* **472**: 115–119.
29. Gaubert H, Sanchez DH, Drost H-G, Paszkowski J (2017) Developmental Restriction of Retrotransposition Activated in Arabidopsis by Environmental Stress. *Genetics* **207**: 813–821.
30. Tenaillon MI, Hollister JD, Gaut BS (2010) A triptych of the evolution of plant transposable elements. *Trends Plant Sci* **15**: 471–478.
31. Sato S, Tabata S, Hirakawa H, Asamizu E, Shirasawa K, Isobe S, Kaneko T, Nakamura Y, Shibata D, Aoki K, et al. (2012) The tomato genome sequence provides insights into fleshy fruit evolution. *Nature* **485**: 635–641.
32. Xiao H, Jiang N, Schaffner E, Stockinger EJ, van der Knaap E (2008) A Retrotransposon-Mediated Gene Duplication Underlies Morphological Variation of Tomato Fruit. *Science (80-)* **319**: 1527–1530.
33. Jiang N, Gao D, Xiao H, van der Knaap E (2009) Genome organization of the tomato sun locus and characterization of the unusual retrotransposon Rider. *Plant J* **60**: 181–193.
34. Rodríguez GR, Muños S, Anderson C, Sim S-C, Michel A, Causse M, Gardener BBM, Francis D, van der Knaap E (2011) Distribution of SUN, OVATE, LC, and FAS in the tomato germplasm and the relationship to fruit shape diversity. *Plant Physiol* **156**: 275–285.
35. Reynard GB (1961) New source of the j2 gene governing Jointless pedicel in tomato. *Science (80-)* **134**: 2102.
36. Rick CM (1956) A new jointless gene from the Galapagos L. pimpinellifolium. *TGC Rep* 23.
37. Rick CM (1956) Genetic and Systematic Studies on Accessions of Lycospersicon from the Galapagos Islands. *Am J Bot* **43**: 687.
38. Soyk S, Lemmon ZH, Oved M, Fisher J, Liberatore KL, Park SJ, Goren A, Jiang K, Ramos A, van der Knaap E, et al. (2017) Bypassing

Negative Epistasis on Yield in Tomato Imposed by a Domestication Gene. *Cell* **169**: 1142–1155.e12.

39. Fray RG, Grierson D (1993) Identification and genetic analysis of normal and mutant phytoene synthase genes of tomato by sequencing, complementation and co-suppression. *Plant Mol Biol* **22**: 589–602.
40. Jiang N, Visa S, Wu S, Knaap E Van Der (2012) *Rider Transposon Insertion and Phenotypic Change in Tomato*. Springer Berlin Heidelberg, Berlin, Heidelberg.
41. Busch BL, Schmitz G, Rossmann S, Piron F, Ding J, Bendahmane A, Theres K (2011) Shoot Branching and Leaf Dissection in Tomato Are Regulated by Homologous Gene Modules. *Plant Cell* **23**: 3595–3609.
42. Brown JC, Chaney RL, Ambler JE (1971) A New Tomato Mutant Inefficient in the Transport of Iron. *Physiol Plant* **25**: 48–53.
43. Ling H-Q, Bauer P, Bereczky Z, Keller B, Ganal M (2002) The tomato fer gene encoding a bHLH protein controls iron-uptake responses in roots. *Proc Natl Acad Sci U S A* **99**: 13938–13943.
44. Cheng X, Zhang D, Cheng Z, Keller B, Ling H-Q (2009) A New Family of Ty1-copia-Like Retrotransposons Originated in the Tomato Genome by a Recent Horizontal Transfer Event. *Genetics* **181**: 1183–1193.
45. Wang Y, Diehl A, Wu F, Vrebalov J, Giovannoni J, Siepel A, Tanksley SD (2008) Sequencing and comparative analysis of a conserved syntenic segment in the Solanaceae. *Genetics* **180**: 391–408.
46. Gilbert C, Feschotte C (2018) Horizontal acquisition of transposable elements and viral sequences: patterns and consequences. *Curr Opin Genet Dev* **49**: 15–24.
47. Gouil Q, Baulcombe DC (2016) DNA Methylation Signatures of the Plant Chromomethyltransferases. *PLoS Genet* **12**: 1–17.
48. Tanksley SD, Ganal MW, Prince JP, De Vicente MC, Bonierbale MW, Broun P, Fulton TM, Giovannoni JJ, Grandillo S, Martin GB, et al. (1992) High density molecular linkage maps of the tomato and potato genomes. *Genetics* **132**: 1141–1160.
49. Catoni M, Griffiths J, Becker C, Zabet NR, Bayon C, Dapp M, Lieberman□Lazarovich M, Weigel D, Paszkowski J (2017) DNA sequence properties that predict susceptibility to epiallelic switching.

1032 *EMBO J* **36**: 617–628.
1033 50. Catoni M, Tsang JM, Greco AP, Zabet NR (2018) DMRcaller: a versatile
1034 R/Bioconductor package for detection and visualization of differentially
1035 methylated regions in CpG and non-CpG contexts. *Nucleic Acids Res*
1036 1–11.
1037 51. Lawrence M, Huber W, Pagès H, Aboyoun P, Carlson M, Gentleman R,
1038 Morgan MT, Carey VJ (2013) Software for Computing and Annotating
1039 Genomic Ranges. *PLoS Comput Biol* **9**: 1–10.
1040 52. Pruitt KD, Tatusova T, Maglott DR (2007) NCBI reference sequences
1041 (RefSeq): a curated non-redundant sequence database of genomes,
1042 transcripts and proteins. *Nucleic Acids Res* **35**: D61-5.
1043 53. Drost H-G, Paszkowski J (2017) Biomartr: genomic data retrieval with
1044 R. *Bioinformatics* **33**: 1216–1217.
1045 54. Fernandez-Pozo N, Menda N, Edwards JD, Saha S, Tecle IY, Strickler
1046 SR, Bombarely A, Fisher-York T, Pujar A, Foerster H, et al. (2015) The
1047 Sol Genomics Network (SGN)—from genotype to phenotype to
1048 breeding. *Nucleic Acids Res* **43**: D1036–D1041.
1049 55. Lowe TM, Eddy SR (1996) TRNAscan-SE: A program for improved
1050 detection of transfer RNA genes in genomic sequence. *Nucleic Acids*
1051 *Res* **25**: 955–964.
1052 56. Michaud M, Cognat V, Duchêne AM, Maréchal-Drouard L (2011) A
1053 global picture of tRNA genes in plant genomes. *Plant J* **66**: 80–93.
1054 57. Finn RD, Coggill P, Eberhardt RY, Eddy SR, Mistry J, Mitchell AL,
1055 Potter SC, Punta M, Qureshi M, Sangrador-Vegas A, et al. (2016) The
1056 Pfam protein families database: towards a more sustainable future.
1057 *Nucleic Acids Res* **44**: D279–D285.
1058 58. Rognes T, Flouri T, Nichols B, Quince C, Mahé F (2016) VSEARCH: a
1059 versatile open source tool for metagenomics. *PeerJ* **4**: e2584.
1060 59. Altschul SF, Gish W, Miller W, Myers EW, Lipman DJ (1990) Basic local
1061 alignment search tool. *J Mol Biol* **215**: 403–410.
1062 60. Galindo-González L, Mhiri C, Deyholos MK, Grandbastien MA (2017)
1063 LTR-retrotransposons in plants: Engines of evolution. *Gene* **626**: 14–25.
1064 61. Yang T, Poovaiah BW (2002) A calmodulin-binding/CGCG box DNA-
1065 binding protein family involved in multiple signaling pathways in plants.

J Biol Chem **277**: 45049–45058.

62. Abe H, Urao T, Ito T, Seki M, Shinozaki K, Yamaguchi-Shinozaki K (2003) Arabidopsis AtMYC2 (bHLH) and AtMYB2 (MYB) function as transcriptional activators in abscisic acid signaling. *Plant Cell* **15**: 63–78.

63. Yang A, Dai X, Zhang W-H (2012) A R2R3-type MYB gene, OsMYB2, is involved in salt, cold, and dehydration tolerance in rice. *J Exp Bot* **63**: 2541–2556.

64. Gómez-Porras JL, Riaño-Pachón D, Dreyer I, Mayer JE, Mueller-Roeber B (2007) Genome-wide analysis of ABA-responsive elements ABRE and CE3 reveals divergent patterns in Arabidopsis and rice. *BMC Genomics* **8**: 260.

65. Timmerhaus G, Hanke ST, Buchta K, Rensing SA (2011) Prediction and validation of promoters involved in the abscisic acid response in physcomitrella patens. *Mol Plant* **4**: 713–729.

66. Vishwakarma K, Upadhyay N, Kumar N, Yadav G, Singh J, Mishra RK, Kumar V, Verma R, Upadhyay RG, Pandey M, et al. (2017) Abscisic Acid Signaling and Abiotic Stress Tolerance in Plants: A Review on Current Knowledge and Future Prospects. *Front Plant Sci* **08**: 1–12.

67. Sagi M, Fluhr R, Lips SH (1999) Aldehyde oxidase and xanthine dehydrogenase in a flacca tomato mutant with deficient abscisic acid and wilty phenotype. *Plant Physiol* **120**: 571–578.

68. Parry AD, Neill SJ, Horgan R (1988) Xanthoxin levels and metabolism in the wild-type and wilty mutants of tomato. *Planta* **173**: 397–404.

69. Burbidge A, Grieve TM, Jackson A, Thompson A, Mccarty DR, Taylor IB (1999) Characterization of the ABA-deficient tomato mutant notabilis and its relationship with maize Vp14. *Plant J* **17**: 427–431.

70. Harrison E, Burbidge A, Okyere JP, Thompson AJ, Taylor IB (2011) Identification of the tomato ABA-deficient mutant sitiens as a member of the ABA-aldehyde oxidase gene family using genetic and genomic analysis. *Plant Growth Regul* **64**: 301–309.

71. Maruyama KY, Todaka DA, Mizoi JU, Yoshida TA, Kidokoro SA, Matsukura SA, Takasaki HI, Sakurai TE, Yamamoto YOY, Yoshiwara KY (2012) Identification of Cis -Acting Promoter Elements in Cold- and Dehydration- Induced Transcriptional Pathways in Arabidopsis , Rice ,

and Soybean. *DNA Res* **19**: 37–49.

72. Perlman PS, Boeke JD (2004) Ring around the retroelement. *Science* **303**: 182–184.

73. Kilzer JM, Stracker T, Beitzel B, Meek K, Weitzman M, Bushman FD (2003) Roles of host cell factors in circularization of retroviral DNA. *Virology* **314**: 460–467.

74. Li L, Olvera JM, Yoder KE, Mitchell RS, Butler SL, Lieber M, Martin SL, Bushman FD (2001) Role of the non-homologous DNA end joining pathway in the early steps of retroviral infection. *EMBO J* **20**: 3272–3281.

75. Flavell AJ, Ish-Horowicz D (1981) Extrachromosomal circular copies of the eukaryotic transposable element copia in cultured Drosophila cells. *Nature* **292**: 591–595.

76. Flavell AJ, Ish-horowicz D (1981) Extrachromosomal circular copies of the eukaryotic transposable element copia in cultured Drosophila cells. *Nature* **292**: 591–595.

77. Tam SM, Causse M, Garchery C, Burck H, Mhiri C, Grandbastien M-A (2007) The distribution of copia-type retrotransposons and the evolutionary history of tomato and related wild species. *J Evol Biol* **20**: 1056–1072.

78. Yin H, Liu J, Xu Y, Liu X, Zhang S, Ma J, Du J (2013) TARE1, a Mutated Copia-Like LTR Retrotransposon Followed by Recent Massive Amplification in Tomato. *PLoS One* **8**: e68587.

79. Wang Y, Tang X, Cheng Z, Mueller L, Giovannoni J, Tanksley SD (2006) Euchromatin and pericentromeric heterochromatin: comparative composition in the tomato genome. *Genetics* **172**: 2529–2540.

80. Cavrak V V., Lettner N, Jamge S, Kosarewicz A, Bayer LM, Mittelsten Scheid O (2014) How a Retrotransposon Exploits the Plant's Heat Stress Response for Its Activation. *PLoS Genet* **10**: e1004115.

81. Strand DJ, Mcdonald JF (1985) Copia is transcriptionally responsive to environmental stress. *Nucleic Acids Res* **13**: 4401–4410.

82. Li Z, Peng R, Tian Y, Han H, Xu J, Yao Q (2016) Genome-Wide Identification and Analysis of the MYB Transcription Factor Superfamily in Solanum lycopersicum. *Plant Cell Physiol* **57**: 1657–1677.

1134 83. Seo PJ, Xiang F, Qiao M, Park J-Y, Lee YN, Kim S-G, Lee Y-H, Park
1135 WJ, Park C-M (2009) The MYB96 transcription factor mediates abscisic
1136 acid signaling during drought stress response in Arabidopsis. *Plant*
1137 *Physiol* **151**: 275–289.
1138 84. Zhu N, Cheng S, Liu X, Du H, Dai M, Zhou D-X, Yang W, Zhao Y (2015)
1139 The R2R3-type MYB gene OsMYB91 has a function in coordinating
1140 plant growth and salt stress tolerance in rice. *Plant Sci* **236**: 146–156.
1141 85. Sugimoto K, Takeda S, Hirochika H (2000) MYB-related transcription
1142 factor NtMYB2 induced by wounding and elicitors is a regulator of the
1143 tobacco retrotransposon Tto1 and defense-related genes. *Plant Cell* **12**:
1144 2511–2528.
1145 86. Corem S, Doron-Faigenboim A, Jouffroy O, Maumus F, Arazi T, Bouché
1146 N (2018) Redistribution of CHH Methylation and Small Interfering RNAs
1147 across the Genome of Tomato ddm1 Mutants. *Plant Cell* **30**:
1148 tpc.00167.2018.
1149 87. Kravchik M, Damodharan S, Stav R, Arazi T (2014) Generation and
1150 characterization of a tomato DCL3-silencing mutant. *Plant Sci* **221**–**222**:
1151 81–89.
1152 88. Panda K, Ji L, Neumann DA, Daron J, Schmitz RJ, Slotkin RK (2016)
1153 Full-length autonomous transposable elements are preferentially
1154 targeted by expression-dependent forms of RNA-directed DNA
1155 methylation. *Genome Biol* **17**: 170.
1156 89. McCue AD, Panda K, Nuthikattu S, Choudury SG, Thomas EN, Slotkin
1157 RK (2015) ARGONAUTE 6 bridges transposable element mRNA-
1158 derived siRNAs to the establishment of DNA methylation. *EMBO J* **34**:
1159 20–35.
1160 90. Nuthikattu S, McCue AD, Panda K, Fultz D, DeFraia C, Thomas EN,
1161 Slotkin RK (2013) The Initiation of Epigenetic Silencing of Active
1162 Transposable Elements Is Triggered by RDR6 and 21-22 Nucleotide
1163 Small Interfering RNAs. *Plant Physiol* **162**: 116–131.
1164 91. Cuerda-Gil D, Slotkin RK (2016) Non-canonical RNA-directed DNA
1165 methylation. *Nat Plants* **2**: 16163.
1166 92. Matzke M a, Mosher R a (2014) RNA-directed DNA methylation: an
1167 epigenetic pathway of increasing complexity. *Nat Rev Genet* **15**: 394–

1168 408.
1169 93. Deaton A, Bird A (2011) CpG islands and the regulation of transcription.
1170 *Genes Dev* **25**: 1010–1022.
1171 94. Ashikawa I (2001) Gene-associated CpG islands in plants as revealed
1172 by analyses of genomic sequences. *Plant J* **26**: 617–625.
1173

FIGURE LEGENDS

Figure 1: Chromosomal location and phylogenetic relationships of *de novo* annotated full-length *Rider* elements

(A) Chromosomal positions of 71 *de novo* annotated full-length *Rider* elements in the SL3.0 genome. *Rider* copies are marked as coloured vertical bars, with colours reflecting similarity between LTRs for each element. Dark grey areas delimitate the centromeres, light grey pericentromeric heterochromatin, and white euchromatin. (B) Phylogenetic relationship of the 71 *de novo* annotated *Rider* elements. The phylogenetic tree was constructed using the neighbour-joining method on nucleotide sequences of each *Rider* copy.

Figure 2: *Rider* activation is stimulated by drought and ABA

(A) Identification of *cis*-regulatory elements (CREs) within *Rider* LTRs. *Rider* LTR U3, R and U5 regions are marked, as well as neighbouring Target Site Duplication (TSD) and Primer Binding Site (PBS) sequences. CREs are marked as coloured vertical bars; their bp positions are given in brackets. (B-C) Quantification of *Rider* RNA levels by RT-qPCR in tomato seedlings after (B) drought stress or (C) mannitol and NaCl treatments. Histograms show normalized expression +/- SEM from two to three biological replicates. **P*<0.05, Student's *t*-test. (D) Quantification of *Rider* RNA levels by RT-qPCR in leaves of drought-stressed tomato wild-type plants, *flc*, *not* and *sit* mutants. Histograms show normalized expression +/- SEM from two biological replicates. **P*<0.05 denotes difference compared to wild-type control; $^{\#}$*P*<0.05 denotes difference compared to wild-type drought plants, Student's *t*-test. (E) Quantification of *Rider* RNA levels by RT-qPCR in tomato seedlings after ABA treatment. Histograms show normalized expression +/- SEM from two to three biological replicates. **P*<0.05, ****P*<0.001, Student's *t*-test.

Figure 3: Accumulation of *Rider* transcripts in tomato plants deficient in epigenetic regulation

(A) Quantification of *Rider* RNA levels by RT-qPCR in tomato seedlings treated with 5-azacytidine and/or ABA. Histograms show normalized expression +/- SEM from two to three biological replicates. **P*<0.05, Student's *t*-test.
(B) Abundance of siRNAs at *Rider* elements in wild type, *slnrpd1* and *slnrpe1*. Data are expressed as siRNA reads per kb per million mapped reads and represent average normalized siRNA counts on *Rider* elements +/- SD from 71 *de novo* annotated *Rider* copies. ****P*<0.001, Student's *t*-test. (C) Quantification of *Rider* RNA by RT-qPCR in *slnrpd1* and *slnrpe1* compared to wild type. Histograms show normalized expression +/- SEM from two to four biological replicates. **P*<0.05, Student's *t*-test.

Figure 4: Accumulation of *Rider* extrachromosomal DNA in drought-stressed plants and in *slnrpd1* and *slnrpe1* mutants

(A) Assay by inverse PCR of *Rider* extrachromosomal circular DNA in drought-stressed wild-type plants and stressed *sit* mutants. Primer localization shown on the left (grey bar: *Rider* element, black box: LTR, arrowheads: PCR primers). Upper gel: specific PCR amplification of *Rider* circles after DNase treatment, lower gel: control PCR for *Rider* detection without DNase treatment. (B) Quantification of *Rider* DNA copy number, including both chromosomal and extrachromosomal copies, by qPCR in leaves of tomato plants subjected to drought-stress. Histograms show normalized expression +/- SEM from two to three biological replicates. **P*<0.05, Student's *t*-test. (C) Assay by inverse PCR of *Rider* extrachromosomal circular DNA in *slnrpd1* and *slnrpe1* leaves. Upper gel: PCR amplification of *Rider* circles after DNase treatment, lower gel: control PCR for *Rider* detection without DNase treatment. (D) Quantification of *Rider* DNA copy number, including both chromosomal and extrachromosomal copies, by qPCR in *slnrpd1* and *slnrpe1* leaves. Histograms show normalized expression +/- SEM from two biological replicates. **P*<0.05, Student's *t*-test. (E) Quantification of CHH DNA

1242 methylation levels at *Rider_08_3* and *Rider_07_2* in wild type, *slnrpd1* and
1243 *slnrpe1*. Levels expressed as % of methylated CHH sites. (F) Normalized
1244 siRNA count of 21-22-nt and 24-nt siRNAs at *Rider_08_3* and *Rider_07_2* in
1245 wild type, *slnrpd1* and *slnrpe1*. Data are expressed as siRNA reads per kb per
1246 million mapped reads.
1247
1248 **Figure 5: Distribution of *Rider* in other *Solanaceae* species**
1249
1250 (A) *In silico* identification of *Rider* elements in *Solanaceae* species based on
1251 the density of high homology BLAST hits over the full-length reference *Rider*
1252 sequence. (B) Alignment length of high homology BLAST hits obtained in (A).
1253 (C) *In silico* identification of *Rider* elements in *Solanaceae* species based on
1254 the density of high homology BLAST hits over the reference *Rider* LTR
1255 sequence. (D) Alignment length of high homology BLAST hits obtained in (C).
1256 Left panels (A) and (C): phylogenetic trees of the species examined.

TABLES

Table 1: Distribution of *de novo* annotated *Rider* elements based on chromatin context

Table 2: Distribution of *de novo* annotated *Rider* elements based on gene proximity

SUPPLEMENTARY FIGURE LEGENDS

Figure S1: Distribution of 71 *de novo* annotated *Rider* elements based on LTR similarity and chromatin context

(A) Age distribution of total *Rider* elements based on LTR similarity and corresponding classes. (B) Age distribution of *Rider* elements inserted in heterochromatic (HC) and euchromatic (EC) regions based on LTR similarity.

Figure S2: *Rider* transcripts levels are unaffected by cold stress

(A-D) Quantification of *SlASR1* RNA levels by RT-qPCR in wild-type tomato seedlings after (A) drought stress (B) mannitol, (C) NaCl or (D) ABA treatments. (E) Quantification of *SlASR1* RNA levels in leaves of drought-stressed tomato wild-type plants, *flc*, *not* and *sit* mutants. (F) Quantification of *SlASR1* RNA levels by RT-qPCR in wild-type tomato seedlings after 5-azacytidine and ABA treatments. (G) Quantification of *Rider* RNA levels by RT-qPCR in wild-type tomato seedlings after cold stress. Histograms show normalized expression +/- SEM from three to five biological replicates.

Figure S3: Distribution of siRNAs and DNA methylation within *Rider* sub-groups

(A) 21-22-nt and (B) 24-nt siRNAs normalized counts at distinct *Rider* sub-groups in wild type, wild type with *CAS9*, *slnrpd1* and *slnrpe1*. *Rider* elements are classified based on LTR similarity (80-95%, 95-98% and 98-100%), while *Rider* (Euchromatin) denotes copies located on euchromatic arms and *Rider* (Heterochromatin) copies located in pericentromeric heterochromatin. Data are expressed as siRNA reads per kb per million mapped reads, and represent average normalized siRNA counts on *Rider* elements +/- SD from *Rider* copies in the sub-group. (C) Quantification of DNA methylation levels in the CG, CHG and CHH contexts at *Rider* in wild type, *slnrpd1* and *slnrpe1*. The levels are averages of DNA methylation (%) in each context over the 71 *de novo* annotated *Rider* copies. (D) Quantification of CHH DNA methylation

levels at *Rider* sub-groups in wild type, *slnrpd1* and *slnrpe1*. The levels are averages of DNA methylation (%) in the CHH context over *Rider* sub-groups.

Figure S4: Distinct *Rider* copies contribute to the production of extrachromosomal circular DNA

Comparison of the LTR nucleotide sequence from *Rider* extrachromosomal circular DNA detected after drought, or in *slnrpd1* (A) or *slnrpe1* (B), with the reference *Rider* LTR using EMBOSS Needle (www.ebi.ac.uk/Tools/psa/emboss_needle/. CREs are marked as coloured boxes. (C) Quantification of CHH DNA methylation levels at LTRs and body of *Rider_08_3* and *Rider_07_2* in wild type, *slnrpd1* and *slnrpe1*. Levels expressed as % of methylated CHH sites. (D-E) Normalized siRNA count of 24-nt (D) and 21-22-nt (E) siRNAs at LTRs and body of *Rider_08_3* and *Rider_07_2* in wild type, *slnrpd1* and *slnrpe1*. Data are expressed as siRNA reads per kb per million mapped reads.

Figure S5: Characterization of *Rider* sub-populations in *Solanaceae* based on LTR sequences

Coverage over reference *Rider* LTR of high homology sequences identified by BLAST in Figure 5C. Sequences classified as “long LTR” were selected by filtering for BLAST hits with alignment lengths between 350-450 bp and >50% sequence and length homology to reference *Rider*. Sequences classified as “short LTR” were selected by filtering for BLAST hits with alignment lengths between 150-300 bp and >50% sequence and length homology to reference *Rider*.

Figure S6: Identification of *Rider* homologs in 14 plant species

In silico identification of *Rider* homologs in 14 plant species based on the density of high homology BLAST hits over the full-length reference *Rider* sequence (left) and alignment length of BLAST hits obtained (right). Species

1333 are ordered by evolutionary distance to *Solanum lycopersicum* from
1334 www.timetree.org, www.genome.jp and Supplementary References.
1335
1336 **Figure S7: Non-*Solanaceae Rider* homologs lack LTR sequence**
1337 **conservation**
1338
1339 *In silico* identification of *Rider* LTR homologs in 14 plant species based on the
1340 density of high homology BLAST hits over the reference *Rider* LTR sequence
1341 only. Species are ordered by evolutionary distance to *Solanum lycopersicum*
1342 from www.timetree.org, www.genome.jp and Supplementary References.
1343

SUPPLEMENTARY TABLES

Table S1: Primers used in this study

Table S2: List of the 110 plant species used for the large-scale *Rider* BLAST search

Table S3: Identification and enrichment analysis of *cis*-regulatory elements in *Rider* LTRs

Table S4: Enrichment analysis of *cis*-regulatory elements in *Rider* LTRs in four *Solanaceae* species

Table S5: *De novo* annotation of LTR retrotransposons in the SL3.0 genome by *LTRpred*

Table S6: Patristic distances between 71 *de novo* annotated *Rider* copies

Table S7: N50 metric for six *Solanaceae* species

SUPPLEMENTARY REFERENCES

Harkess, A. *et al.* The asparagus genome sheds light on the origin and evolution of a young y chromosome. *Nat. Commun.* **8,** (2017).

Zou, C. *et al.* A high-quality genome assembly of quinoa provides insights into the molecular basis of salt bladder-based salinity tolerance and the exceptional nutritional value. *Cell Res.* **27,** 1327–1340 (2017).

a

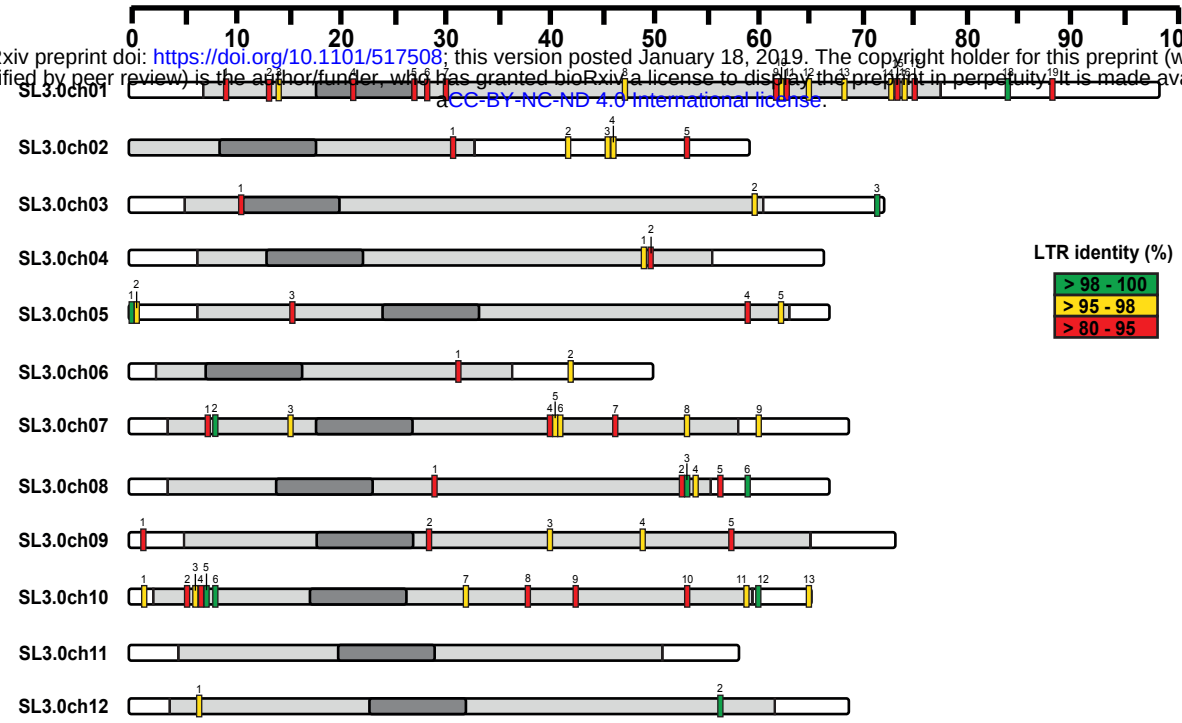

b

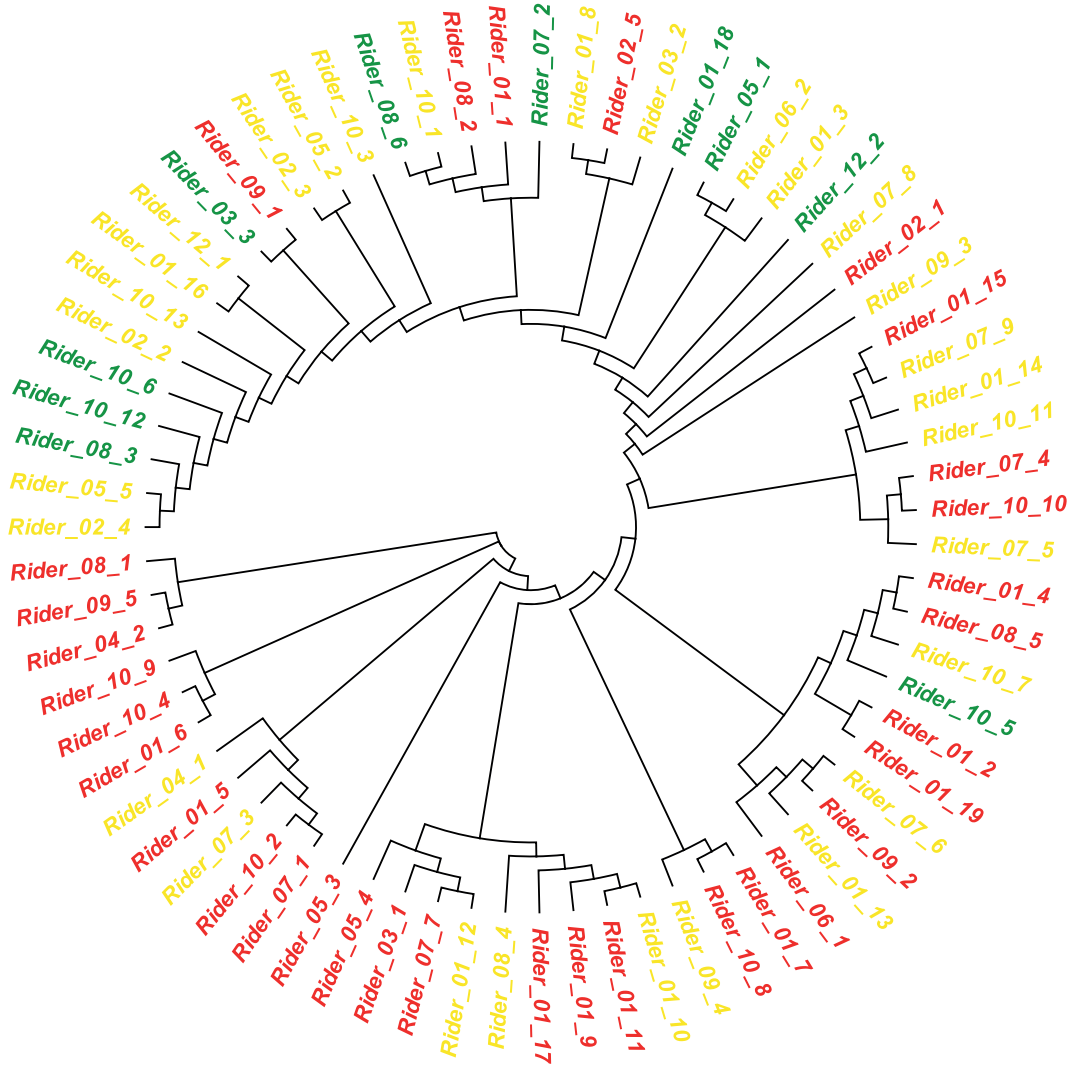

Figure 1

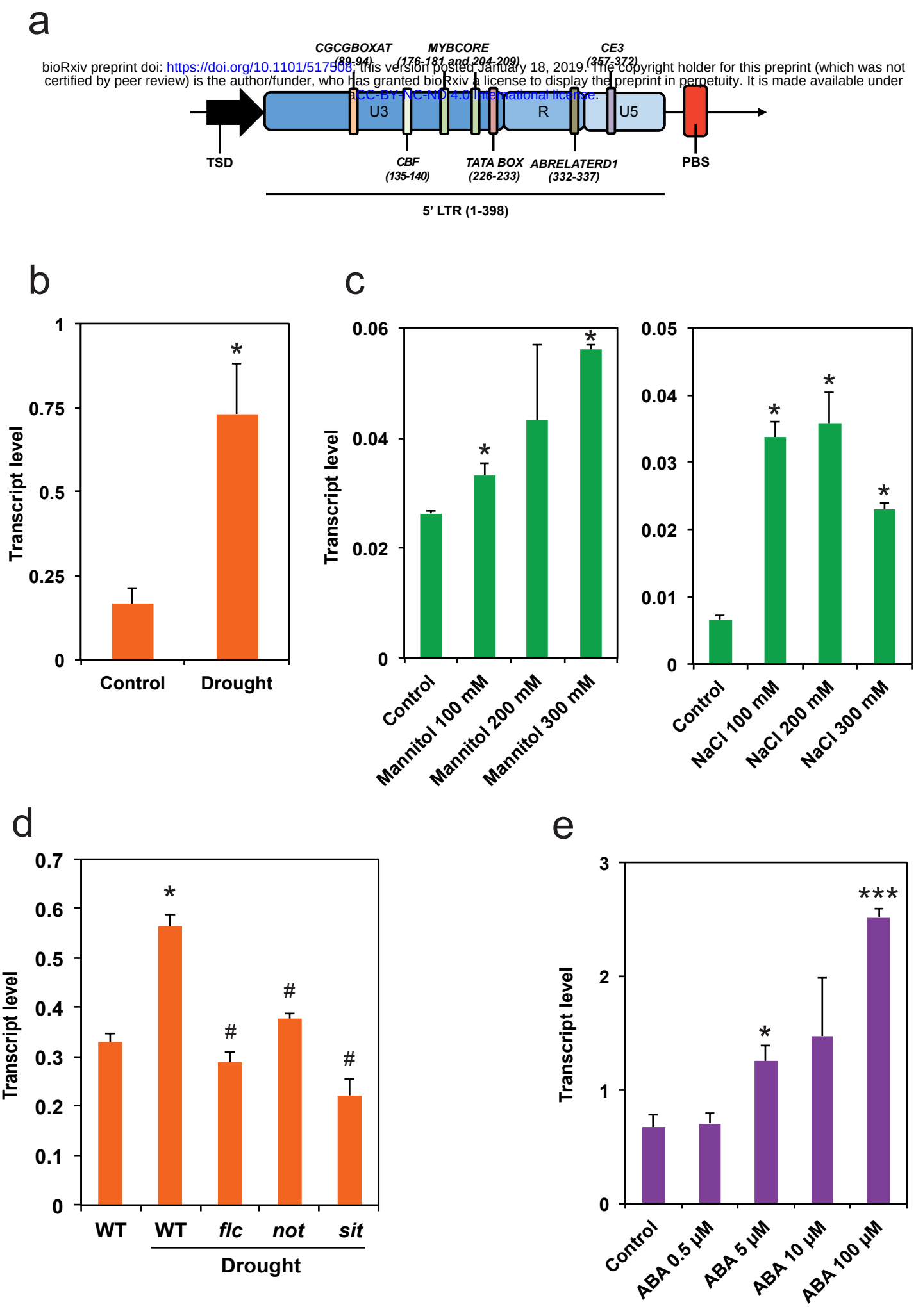

Figure 2

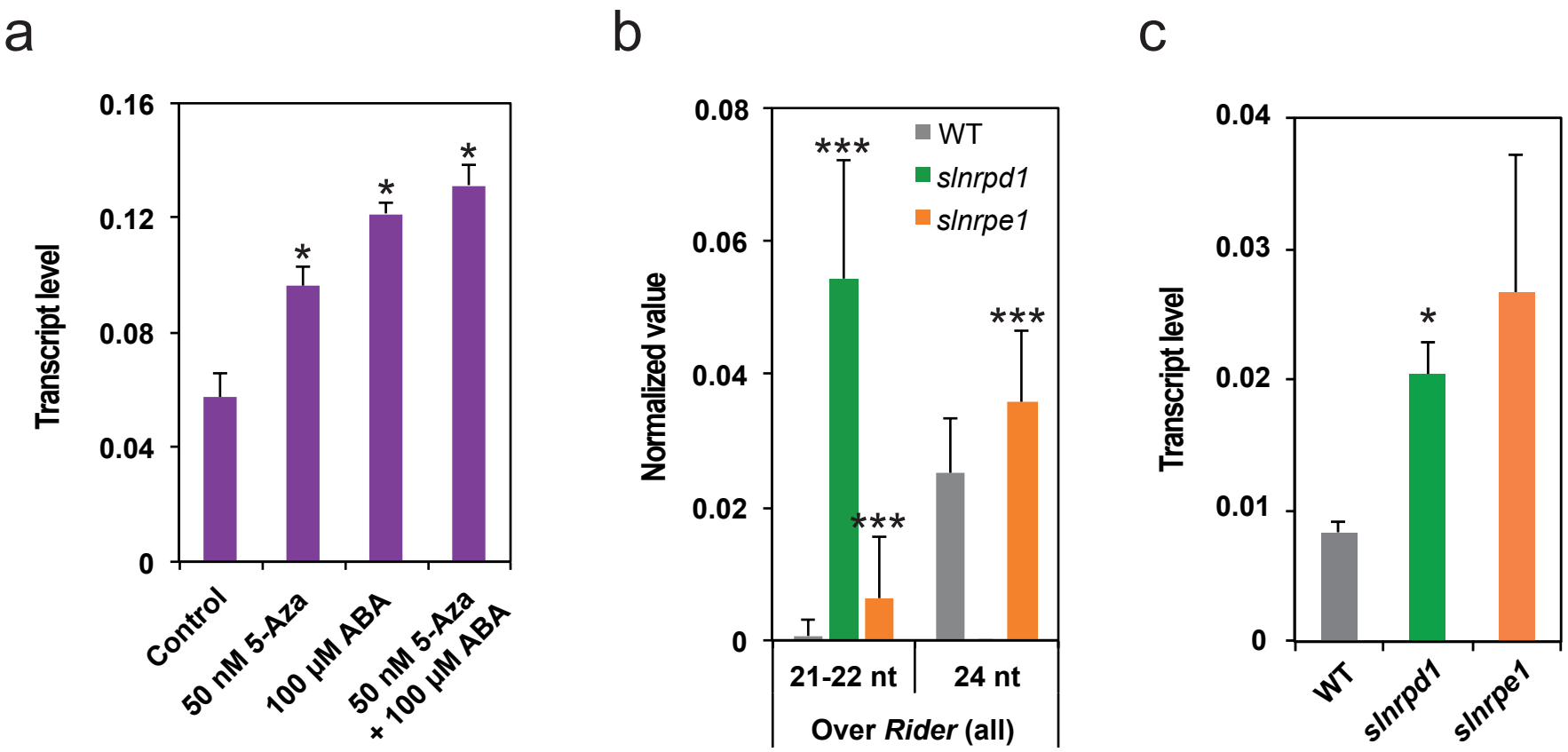
a
b
c
Transcript level
0.16
0.12
0.08
0.04
0
*
*
*
Control
50 nM 5-Aza
100 µM ABA
50 nM 5-Aza
+ 100 µM ABA
Normalized value
0.08
0.06
0.04
0.02
0
***
***
***
WT
slnrpd1
slnrpe1
21-22 nt
24 nt
Over Rider (all)
Transcript level
0.04
0.03
0.02
0.01
0
*
WT
slnrpd1
slnrpe1

Figure 3

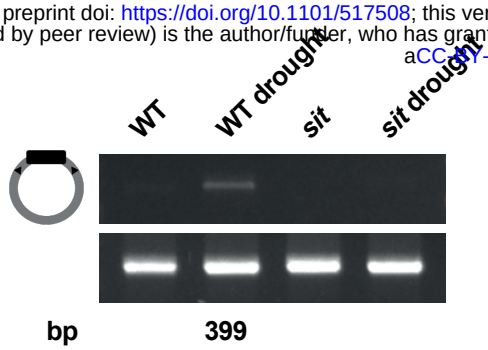

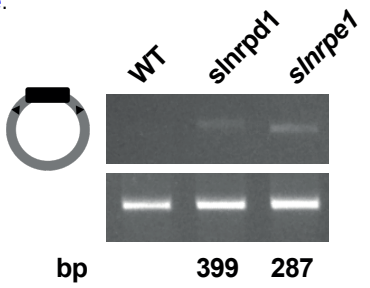

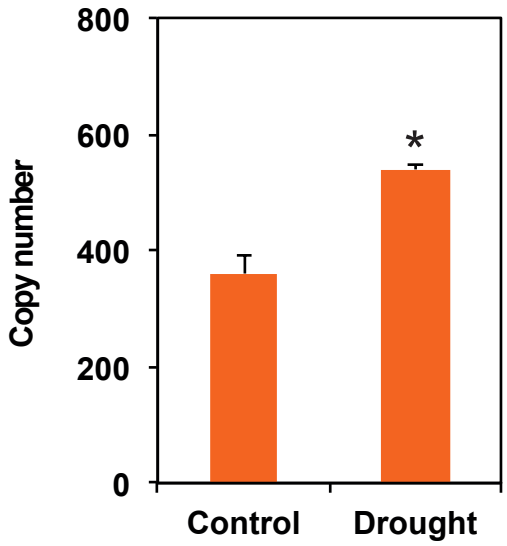

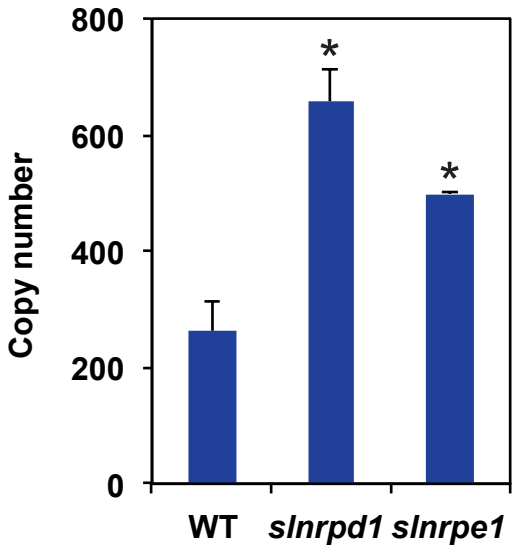

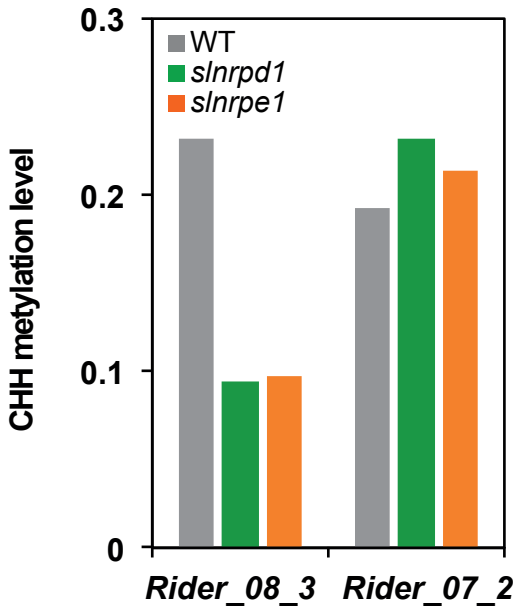

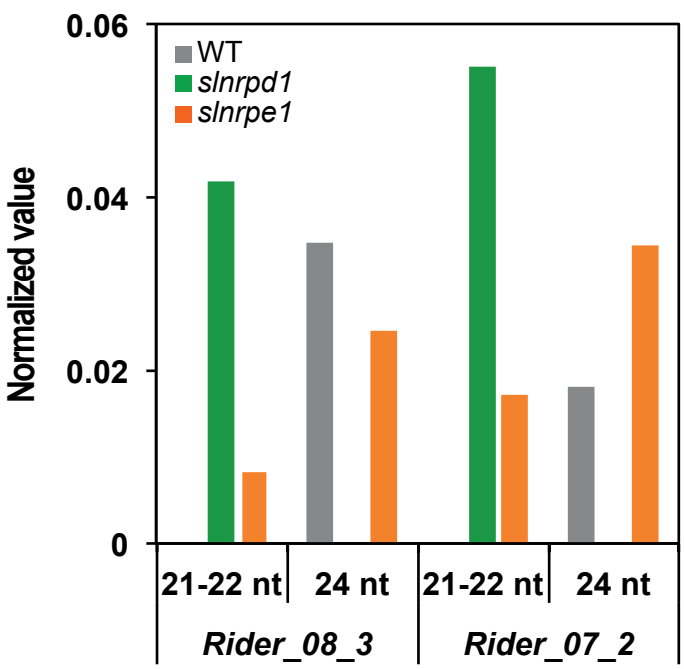

Figure 4

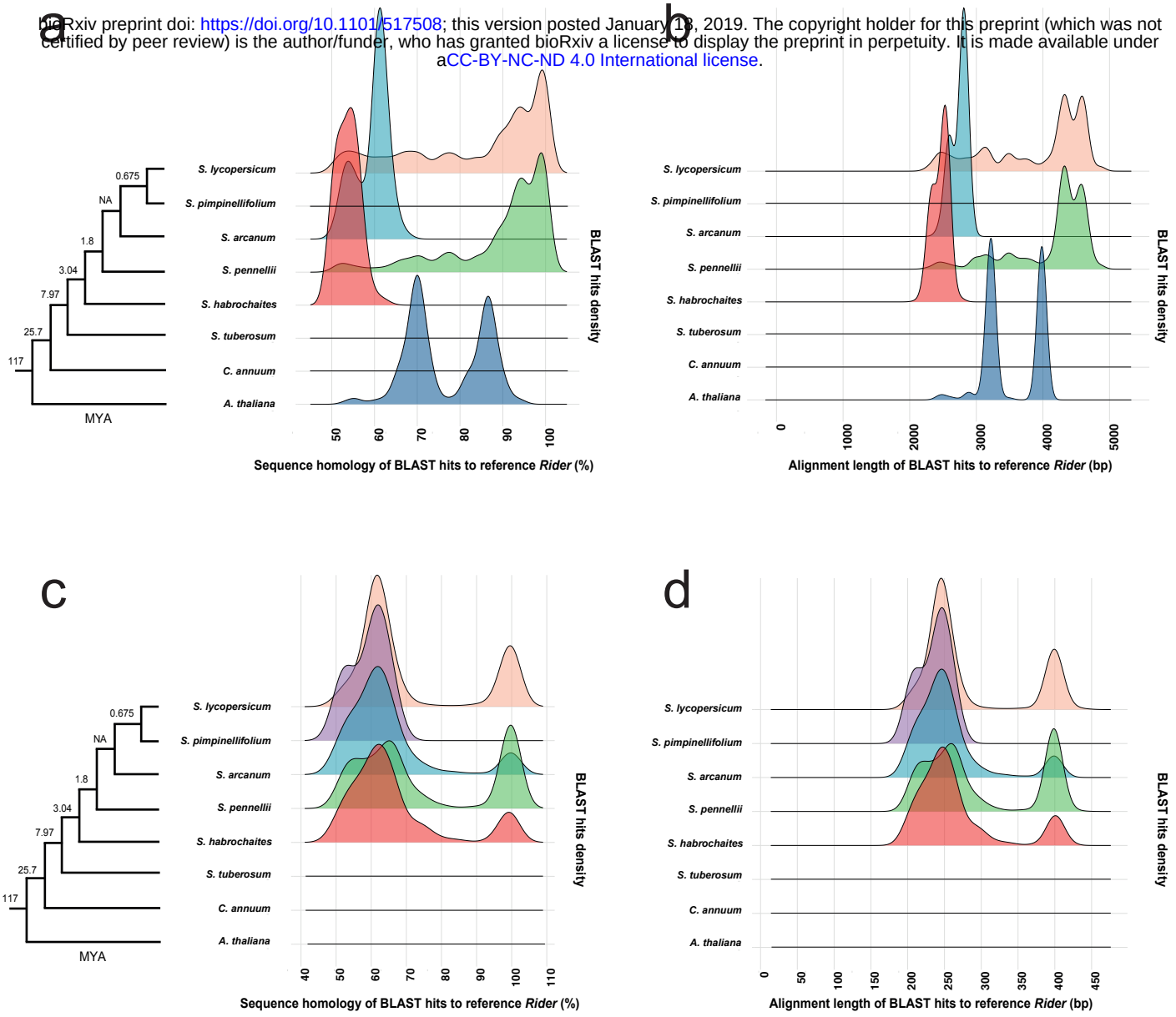

Figure 5

Table 1

	LTR identity (%)			
	98-100	95-98	85-95	Total (%)
Number of elements in chromosome arms	5	6	3	19.7
Number of elements in pericentromeric regions	5	23	29	80.3
Total	10	29	32	100.0

Table 2

	Presence of gene within 2 kb (%)	Number of elements in chromosome arms (%)
Rider_85-95	37.5	9.4
Rider_95-98	48.3	20.7
Rider_98-100	50.0	50